NASA TECHNICAL NOTE

NASA TN D-3945

NASA TN D-3945

EXPERIMENTAL EVALUATION OF SIX ABLATIVE-MATERIAL THRUST CHAMBERS AS COMPONENTS OF STORABLE-PROPELLANT ROCKET ENGINES

by Arthur M. Shinn, Jr.

Lewis Research Center
Cleveland, Ohio

NATIONAL AERONAUTICS AND SPACE ADMINISTRATION • WASHINGTON, D. C. • JUNE 1967

NASA TN D-3945

EXPERIMENTAL EVALUATION OF SIX ABLATIVE-MATERIAL THRUST CHAMBERS AS COMPONENTS OF STORABLE-PROPELLANT ROCKET ENGINES

By Arthur M. Shinn, Jr.

Lewis Research Center
Cleveland, Ohio

NATIONAL AERONAUTICS AND SPACE ADMINISTRATION

For sale by the Clearinghouse for Federal Scientific and Technical Information
Springfield, Virginia 22151 – CFSTI price $3.00

EXPERIMENTAL EVALUATION OF SIX ABLATIVE-MATERIAL THRUST CHAMBERS AS COMPONENTS OF STORABLE-PROPELLANT ROCKET ENGINES

by Arthur M. Shinn, Jr.

Lewis Research Center

SUMMARY

Six ablative-material thrust chambers were tested as components of storable-propellant (nitrogen tetroxide N_2O_4 and a 50-50 blend of unsymmetrical dimethyl hydrazine with hydrazine N_2H_4) rocket engines. The nominal initial nozzle-throat diameters were 7.82 inches (19.8 cm). Engine operating conditions were held constant at a chamber pressure of 100 psia (689 kN/m^2) and an oxidant-to-fuel ratio of 2.0. The six ablative-material thrust chambers provided both material and geometry variables.

A material of high-purity-silica-cloth reinforcement and phenolic resin had greater throat-erosion resistance than one of high-silica-cloth reinforcement and phenolic resin with an elastomer additive or one of graphite-cloth reinforcement and phenolic resin. High-silica-cloth reinforcement used with the fibers oriented 60° downstream relative to the engine centerline had greater throat-erosion resistance than when used as molded 1/2-inch (12.7 mm) squares. An ablative-material chamber section with a 7.66° half-angle of contraction and a tubular throat (ratio of length to diameter L/D = 0.77) provided better throat-erosion resistance than did a chamber section of similar material with a 15° half-angle of contraction and a contoured throat. A full-length ablative-material chamber had better throat-erosion resistance than a chamber of essentially equal overall length but including a water-cooled section ahead of the ablative-material chamber section for run durations greater than 470 seconds. However, the shorter ablative section exhibited a negative area change for the first 410 seconds.

INTRODUCTION

Several present and proposed rocket-engine propulsion systems use ablative materials to provide sacrificial cooling of the thrust chambers. Advantages include simplicity

and potential reliability as well as insensitivity to throttling. In this application, ablative materials are required to provide minimum internal dimensional increase (particularly at the nozzle throat) in order to sustain high engine performance during the required operating life of the chamber and to minimize wall thickness.

Ablative materials are generally tested in high-temperature torches or plasma arcs, but such tests may only provide approximate indications of the capability of a material when subjected to the combustion environment of specific propellant combinations in rocket thrust chambers. Screening tests to identify the better ablative materials in an oxidizing combustion environment have been made utilizing small rocket engines (refs. 1 to 3). Results from the latter studies show relatively great variation in erosion resistance among materials and with test environment. Additional information on experimental studies of small-scale ablative rocket engines may be found in references 4 and 5. Information on subscale and full-scale ablative chamber testing may be found in reference 6.

To evaluate ablative materials for larger scale (compared to refs. 1 to 3) rocket-engine applications, a series of six ablative-material thrust chambers with initial throat diameters of nominally 7.82 inches were tested as components of storable-propellant engines. The results are reported herein. The propellants were nitrogen tetroxide (N_2O_4) and a 50-50 blend of unsymmetrical dimethyl hydrazine with hydrazine. Engine operating conditions were maintained essentially constant by using the same propellant injector throughout the test series and an automatic controller to hold chamber pressure at 100 psia (689 kN/m^2) and oxidant-to-fuel ratio of 2.0. The test series was conducted in an altitude facility at an ambient pressure of about 1.74 psia (12 kN/m^2). Because of a limitation in propellant tankage capacity, the longest continuous firings were of about 100 seconds duration. Four of the ablative-material chambers provided material variables, whereas two provided chamber-geometry variables. The results are presented primarily in terms of nozzle-throat-radius change as a function of accumulative firing time, since throat erosion is considered the most important problem of ablative chambers. The variation of specific impulse, due to throat-radius change, with accumulative firing time is also presented.

APPARATUS

Ablative Materials

The ablative materials from which the thrust chambers were fabricated are given in table I. The chambers have been numbered in the order given in the table, and this number is used herein to identify the chambers. The table lists the material information including reinforcement, fiber orientation, resin, and additive. Wall-layer-thickness information is also given.

TABLE I. - ABLATIVE MATERIALS

Chamber	Reinforcement			Phenolic resin, weight percent	Additive	Weight percent	Layer thickness, in.		Chamber configuration (b)
	Type of cloth	Orientation					Inner	Outer flat wrap[a]	
		Chamber	Throat						
1	Silica	60^{o}	60^{o}	33	---	0	1.0	0.55	A
2	Silica	↓	$\frac{1}{2}$-inch squares (12.7 mm)	33	---	0	↓	↓	↓
3	Silica	↓	60^{o}	33	Elastomer	13	↓	↓	↓
4	Graphite	↓	↓	31	---	0	↓	↓	↓
5	Silica	↓	↓	33	---	0	1.5	0	B
6	Silica	↓	↓	33	---	0	1.5	0	C

[a]Nominal, with same material constituents as inner layer.

[b]Chamber configurations shown in table III.

Chambers 1 through 4 provide ablative-material variables. The reinforcement was high-purity-silica cloth for all but chamber 4 which had graphite cloth. The reinforcement fibers were directed downstream at 60^{o} to the engine centerline in all cases (fig. 10(d), p. 26) except in the throat region of chamber 2, which had molded 1/2-inch squares (12.7 mm) of reinforcement (fig. 9(b), p. 22). Resin was used in about equal amounts in the materials of all chambers, but the resin of chamber 3 also included an elastomer additive to the phenolic.

Chambers 1, 5, and 6 were all made of high-silica-cloth reinforcement and phenolic resin with a fiber orientation of 60^{o} relative to the engine centerline and provided chamber geometry variables, which will be discussed later.

Facility

The investigation was conducted in an altitude chamber (fig. 1). The experimental firings were made at a nominal altitude pressure of 1.74 psia (12 kN/m^2). The engine-exhaust products passed through a water-cooled exhaust collector (which minimized recirculation of the exhaust products in the test chamber), primary and secondary exhaust coolers, and rotating exhausters before being released to the atmosphere approximately 80 feet (24.4 m) above ground level.

The installation in the altitude chamber in shown in figure 2(a). A schematic of the test installation with the pertinent instrumentation is shown in figure 2(b). The engine was supported by flexural plates which were connected to a mounting stand in the test chamber and enabled measurement of thrust by a calibrated load cell (fig. 2(c)). The

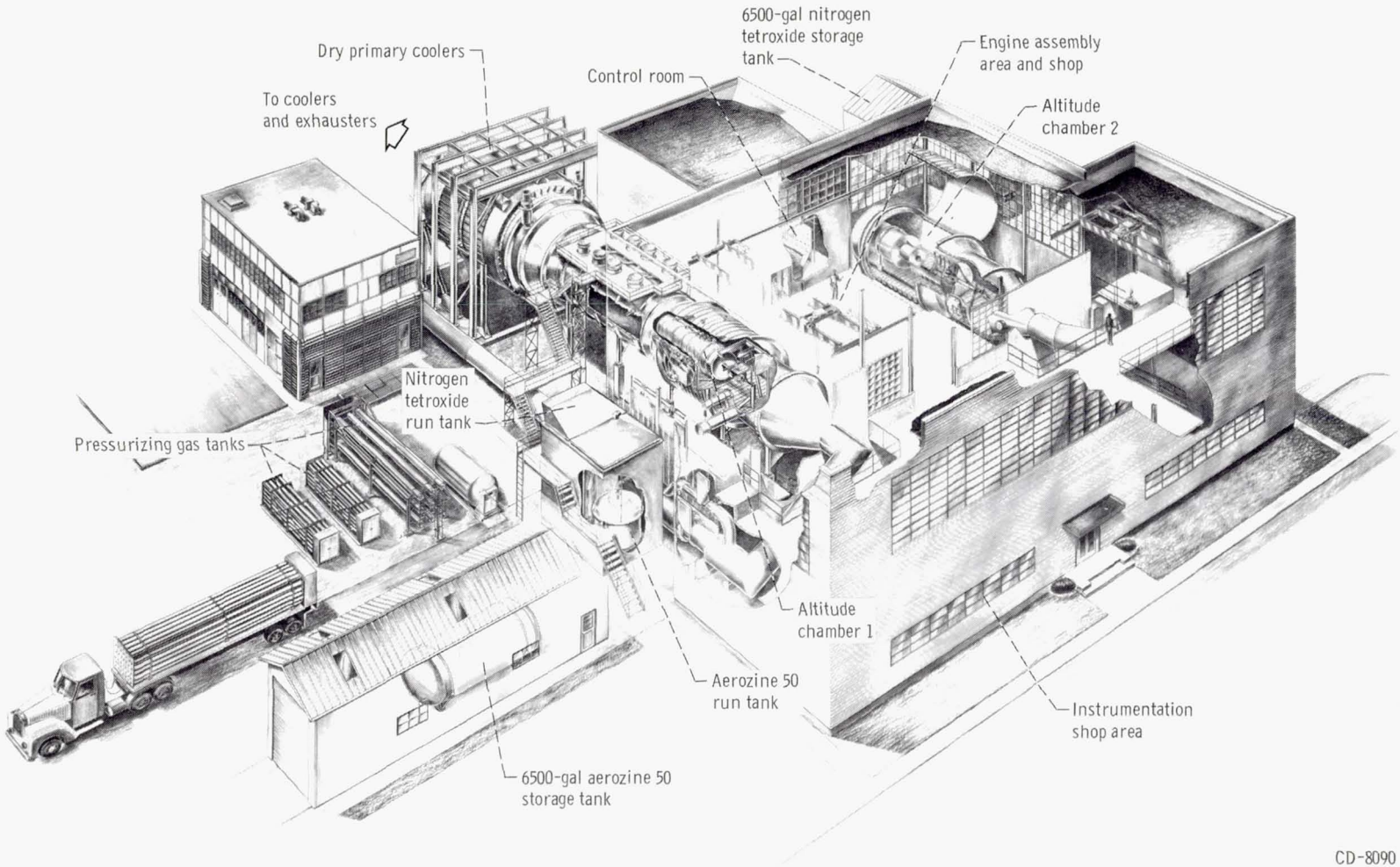

Figure 1. - Altitude facility.

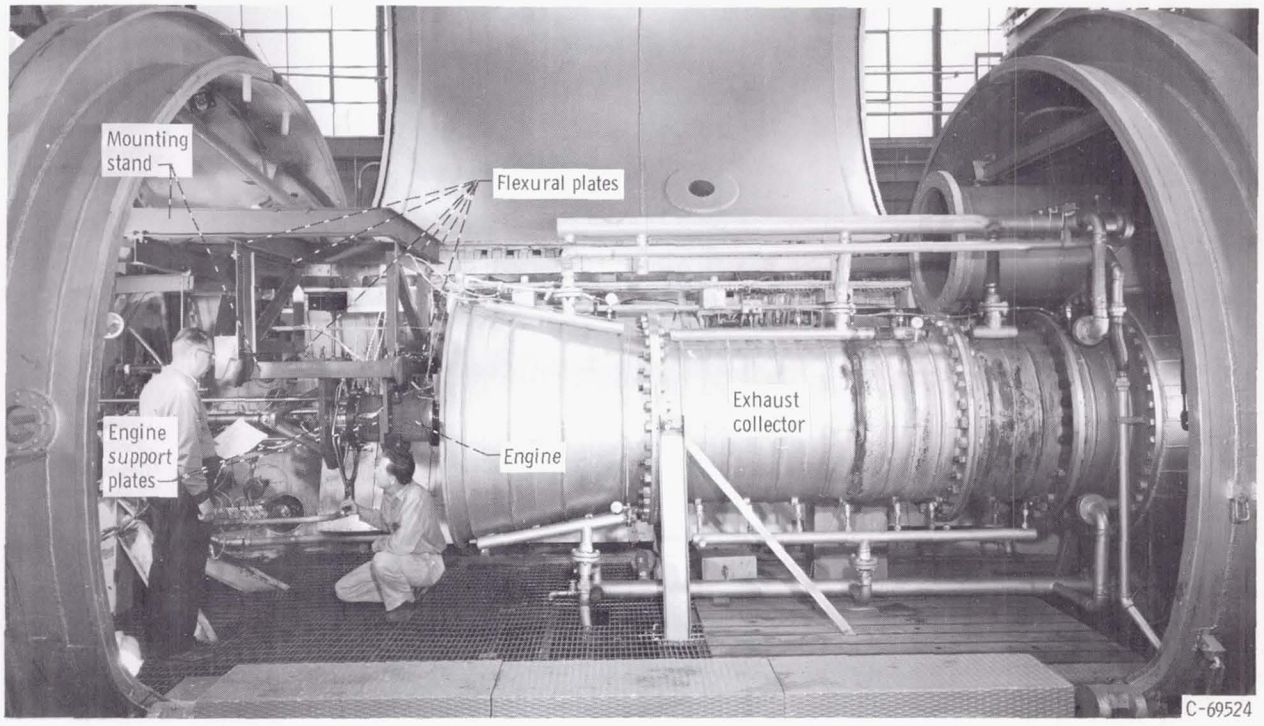

(a) Test chamber and engine.

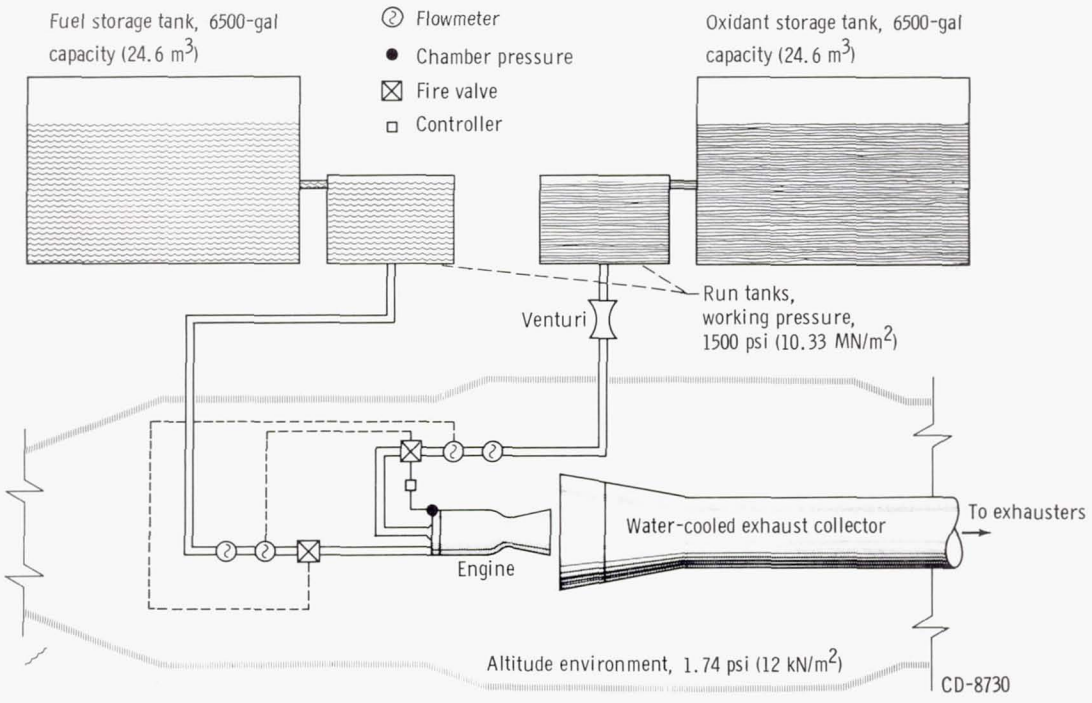

(b) Schematic of altitude test chamber.

Figure 2. - General engine arrangement.

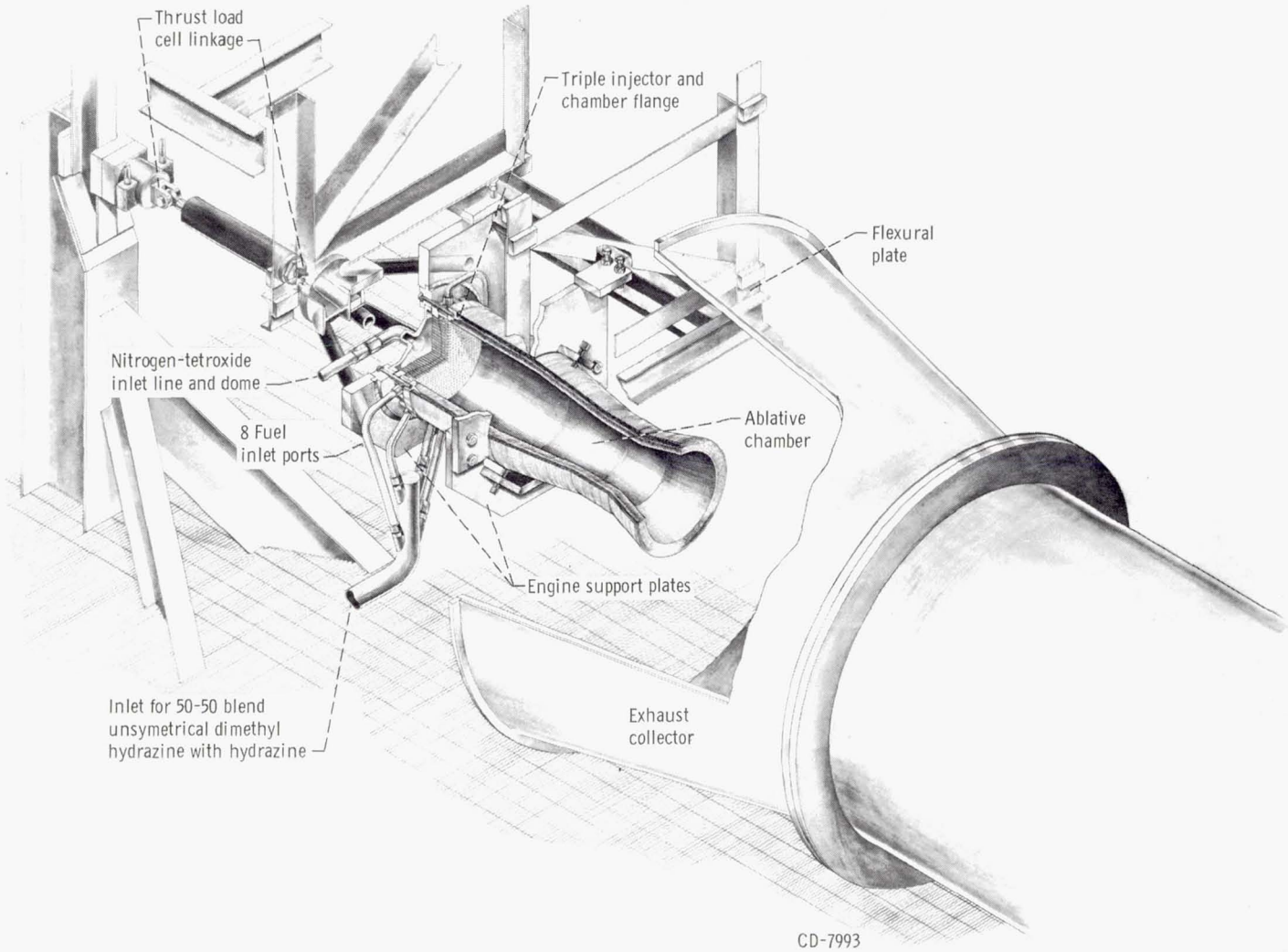

(c) Cutaway view of ablative chamber and injector.

Figure 2. - Concluded.

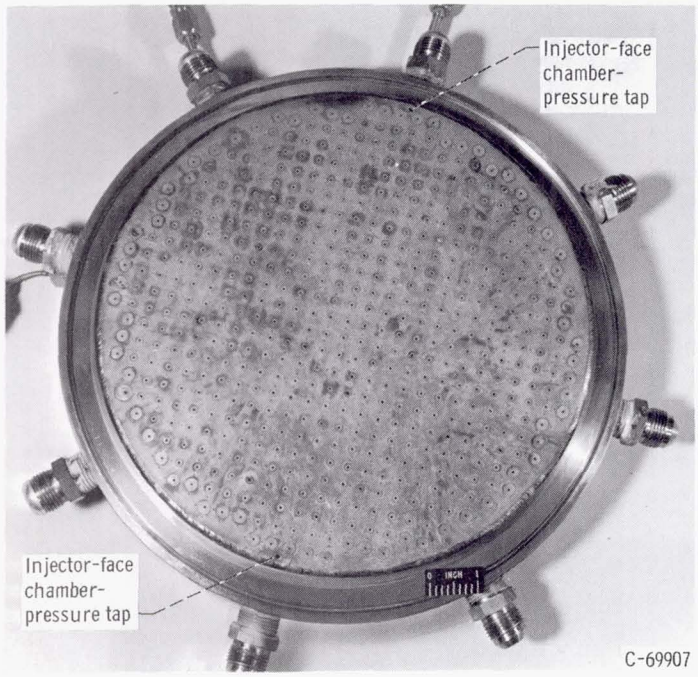

(a) After 313 seconds.

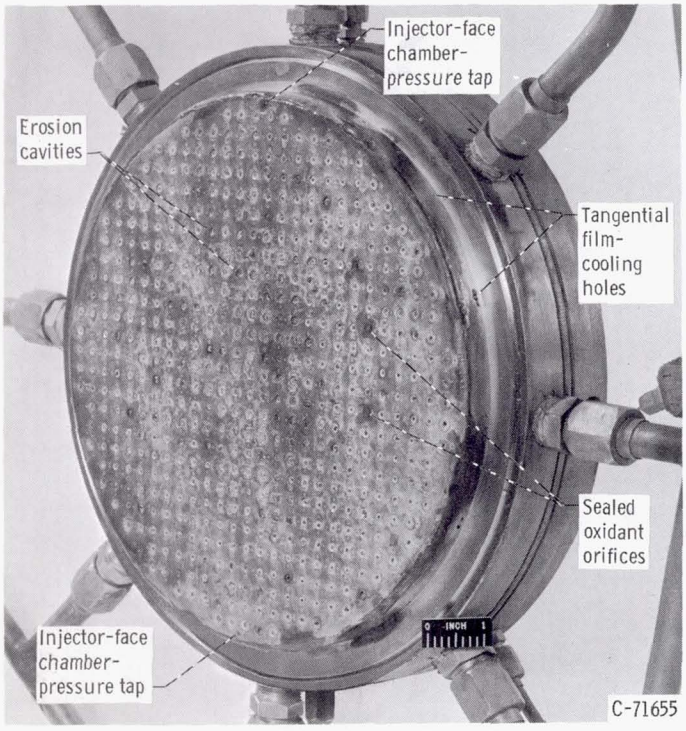

(b) After 3558 seconds.

Figure 3. - Injector.

propellant lines were attached to the engine perpendicular to the thrust axis.

The propellant run tanks were external to the test chamber and were pressurized with nitrogen gas to provide propellant flow to the engine.

Engine

The grid-patterned nickel-faced injector is shown, early in its life, in figure 3(a); additional details are tabulated in table II. The injector included 481 (mutually perpendicular) triplet elements (two fuel streams with an included impingement angle of 30^{o} impinging, at a distance of 0.578 inches (14.7 mm) from the injector face, on a single oxidant stream) surrounded by 72 oxidant and 198 fuel orifices as showerhead elements. The circumferential edge of the injector was film cooled by 2.4 percent of this fuel flow injected tangentially from 16 orifices. The same injector was used throughout the investigation. Water was flowed through the injector periodically to check the uniformity of the flow pattern. Fourteen oxidant tubes were sealed during the course of the investigation in order to prevent spurious oxidant jets, which probably resulted from hole-edge erosion, from impinging on the walls of the combustion chamber. The injector is shown in figure 3(b) a short time before completion of the inves-

TABLE II. - COMPOSITION OF GRID PATTERN

TRIPLET

Injector element	Propellant	Number of holes	Diameter of hole, in. (a)
Triplet (mutually perpendicular)	Oxidant	481	0.035
	Fuel	962	0.018
Showerhead	Oxidant	72	0.035
	Fuel	198	0.018
Tangential perimetrical film cooling	Fuel	8	0.028
		8	0.020

[a]To convert in. to mm, multiply by 25.4.

tigation. The injector-chamber joint was sealed by a stainless-steel O-ring.

The ablative-material thrust-chamber configurations are shown in table III; as indicated previously, the materials are given in table I. The internal diameter of the chambers at the injector face was 10.77 inches (27.4 cm), and the nominal initial throat diameter was 7.82 inches (19.8 cm), providing a contraction ratio of 1.9. Chambers 1 to 4 were of ablative material for their full length (table III, configuration A) and were constructed with an inner layer and an outer flat wrap layer as indicated by table III. Chambers 5 and 6 were shorter ablative chambers (table III, configurations B and C); a 12-inch-long (30.48 cm) water-cooled chamber section was used with these ablative chambers to achieve an overall characteristic length (nominally 45 in. (1.14 m)) comparable to that for chambers 1 to 4. Chambers 1 to 5 included a 7.66° half-angle of contraction and a 6-inch-long (15.2 cm) tubular throat. Chamber 6 included a 15° half-angle of contraction and a contoured throat. The initial nozzle-expansion-area ratio of all chambers was 2.0.

Steel heat-sink chambers with contoured throats (table III, configurations D and E) were used to provide a constant known throat area for evaluation and periodic checking of combustion performance from short-duration firings.

Instrumentation

Sensing. - Strain-gage transducers were used to measure two injector-face chamber pressures, propellant system pressures, test chamber (ambient) pressure, and total pressure at the nozzle throat.

TABLE III. - ORIGINAL COMBUSTION-CHAMBER CONFIGURATIONS

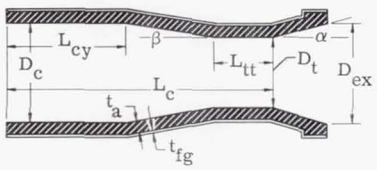

Configuration A. - Full-length tubular-throat ablative chamber.

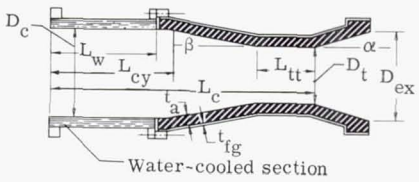

Configuration B. - Short tubular-throat ablative chamber.

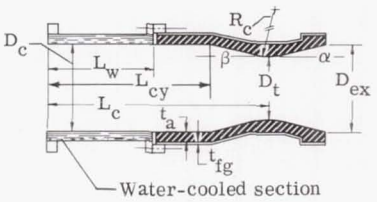

Configuration C. - Short contoured-throat ablative chamber.

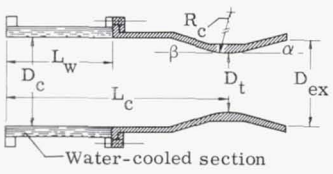

Configuration D. - Short steel heat-sink chamber.

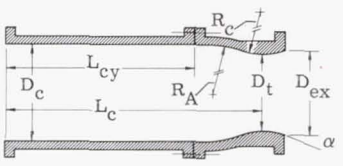

Configuration E. - Full-length steel heat-sink chamber.

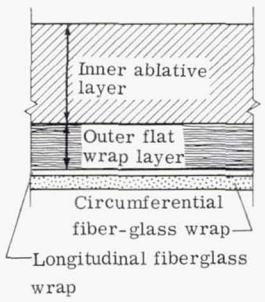

Ablative wall construction

Configuration	D_c, in.	D_t, in. (a)	D_{ex}, in.	L_c, in. (b)	L_{cy}, in.	L_{tt}, in.	L_o^*, in. (a), (b)	L_w, in.	t_a, in.	t_{fg}, in.	R_c, in.	R_A, in.	ϵ_c	ϵ_{ex}	α, deg	β, deg
A	10.77	7.82	11.0	29.9	13.5	6.0	45.1	----	1.5	0.1	----	----	1.9	2.0	15	7.66
B	↓	↓	↓	30.0	13.5	6.0	43.2	12.0	1.5	.1	----	----	↓	↓	↓	7.66
C				24.5	17.0	---	44.5	12.0	1.5	.1	7.82	----				15
D			↓	25.0	----	---	45.4	12.0	---	---	3.9	----		↓		15
E	↓	↓	8.92	28.9	21.0	---	53.0	----	---	---	3.9	7.82	↓	1.3	↓	-----

[a] Nominal.

[b] L_c and L_o are based on distance from injector face to throat.

Thrust was measured by a double-bridge strain-gage load cell.

The fuel flow was measured by two turbine, 2.0-inch-diameter (5.08 cm) flowmeters in series as indicated by figure 2(b). The oxidant flow was measured by two turbine, 2.0-inch-diameter (5.08 cm) flowmeters, and backup data were provided by a verturi meter. Iron constantan thermocouples were used in both propellant lines at the flowmeters to determine propellant temperatures.

Recording and processing. - All electric sensor outputs were digitized, sampled at 4000 samples per second by the central data recording system, and recorded on magnetic tape as the primary data source. Selected sensor outputs were also recorded by high response multichannel oscillograph and strip chart recording instruments for control room data reduction and system monitoring.

The data on magnetic tape were first checked on an oscilloscope display unit and then introduced into the digital computer along with the appropriate calibration constants for conversion and input constants for processing. The output data were printed at every 0.96-second interval for the ablative-chamber runs and 0.096 second for the shorter performance check runs with the steel heat-sink chambers.

PROCEDURE

Testing Techniques

The propellant run tanks were pressurized with nitrogen gas. The automatic closed-loop controller was set to provide the desired chamber pressure of 100 psia (689 kN/m^2) and oxidant-to-fuel ratio, which were to be maintained constant. The altitude chamber pressure was set to 1.74 psia (12 kN/m^2). Short (nominally 6 sec) firings were made periodically throughout the test program, using the steel heat-sink chambers (table III, configurations D and E) to determine the experimental combustion performance level.

One or two consecutive major firings, each of nominally 100-second duration, were made on each ablative chamber as a sequence of runs in a given test period. Minor firings because of aborts and calibration checks varied in length from 0 to 8 seconds. The total accumulative firing time on each engine consisted of the sum of several major and minor firings obtained from several testing periods.

Combustion-Performance Determination

Combustion-performance level was determined, by methods similar to those utilized in reference 7, over the oxidant-to-fuel-ratio range from 1.4 to 2.1, and throughout the

testing time period of 4000 seconds. The primary method of determining the experimental combustion-performance level (vacuum specific-impulse method) consisted of accurately measuring thrust, propellant weight flows, ambient pressure, and expansion area ratio, and experimentally determining the oxidant-to-fuel ratio on the steel heat-sink chambers of configurations D and E (table III). When these parameters, the theoretical equilibrium vacuum specific impulse, and the nozzle thrust coefficient efficiency were known, the combustion performance level could be established. The following equations outline the procedure used. A list of symbols is provided in appendix A.

Vacuum thrust:

$$F_v = F_m + p_o A_{ex} \tag{1}$$

Vacuum specific impulse:

$$I_{v,x} = \frac{F_v}{\dot{W}_t} \tag{2}$$

Vacuum specific impulse efficiency:

$$\eta_{I_{sp,v}} = \frac{I_{v,x}}{I_{v,th\text{-}eq}} \tag{3}$$

Characteristic velocity efficiency:

$$\eta_{c^*,I} = \frac{\eta_{I_v}}{\eta_{C_{F,v}}} = \left(\frac{\eta_{I_v}}{0.968}\right)_{tt} \tag{4}$$

The derivation for the theoretical $\eta_{C_{F,v}}$ appears in appendix B.

An alternative method of establishing the performance level was derived in order to provide an equation that involved the geometrical throat area, injector-face pressure, and the measured flow rate. By this means, the measured flow rate would be directly proportional to geometrical throat area since injector-face chamber pressure was controlled nominally constant.

This method related the injector-face pressure $P_{c,i}$ to the nozzle-throat-inlet total

C-69602

Figure 4. - Throat total-pressure probe.

pressure P_c^* by the parameter φ such that

$$\frac{P_c^*}{P_{c,i}} = \varphi \tag{5}$$

where φ is the conventional momentum pressure loss for cylindrical chambers. A value of $\varphi = 0.946$ was calculated by the method described in reference 7 and was verified experimentally in a steel chamber with a contoured throat using the throat total-pressure probe shown in figure 4. For the contoured throat, isentropic expansion is assumed, and P_c^* at the nozzle entrance becomes P_c^* at the nozzle throat.

For the tubular throat, however, losses are incurred during expansion as a result of the nonisentropic throat section, and P_c at the nozzle entrance is not equivalent to P_c^*. To account for this, a flow coefficient C_d was defined such that the characteristic velocity c*, which is related to combustion efficiency, was not affected by the throat design. Therefore,

$$\eta_{c^*,tc} = \eta_{c^*,tt} = \left(\frac{P_c^* A_t C_d^g}{\dot{W}_t c_{th}^*} \right)_{tt} \tag{6}$$

Subsituting for P_c^* and solving for C_d for the tubular throat give

$$C_{d,\,tt} = \frac{\eta_{c^*,\,tc}\, c^*_{th}}{\left[\dfrac{(\varphi P_{c,\,i})A_t g}{\dot{W}_t}\right]_{tt}} \tag{7}$$

When the value of $\eta_{c^*,\,tc}$ obtained from impulse measurements was used, a value of $C_{d,\,tt}$ was experimentally determined to be 0.977. This same equation was applied to the contoured throat, and $C_{d,\,tc}$ was determined to be 0.994, which agrees with previous investigations noted in references 8 to 10.

This expression also provided the desired relation between the geometrical throat area in terms of measured injector-face pressure and total flow rate.

Throat-Dimension Determination

Three procedures were used throughout the test program in order to determine the throat area and the throat radius change: (1) systematic measurement of the throat diameter with micrometers, (2) mechanical integration of photographs of the throat area, and (3) calculation by the flow equation. Subsequent reference to the three procedures will be made in the abbreviated fashion of micrometer, photograph, and flow equation. Each chamber-throat diameter was measured at 45° intervals with a micrometer after each testing sequence. In the case of the tubular throat chambers, the measurements were made at three axial locations (entrance, middle, and exit of the cylindrical throat).

In most instances, the ablative chambers were alined, and the throat areas were photographed as shown in figures 5(a) and (b). The photographs were enlarged to full scale and printed. Early in the test program, a glossy paper was used for the photographic prints. This paper was later changed, however, to an aeromap paper which has very little dimensional change and provided less slippage for the mechanical integrator or planimeter. The enlarged photographs were mechanically integrated to determine throat area, from which an effective throat radius was calculated.

The flow equation method consisted of the following procedure: (a) measurement of the injector-face pressure $P_{c,\,i}$, which was relatively constant with time, (b) utilization of the experimental nozzle-throat total-pressure correction $\varphi = P^*_c/P_{c,\,i}$, (c) measurement of the propellant flows as a function of time, where $\dot{W}_t(\theta) = \dot{W}_o(\theta) + \dot{W}_f(\theta)$, (d) utilization of the experimentally established combustion performance level $\eta_{c^*,\,I}$, and (e) utilization of the theoretical equilibrium characteristic velocity.

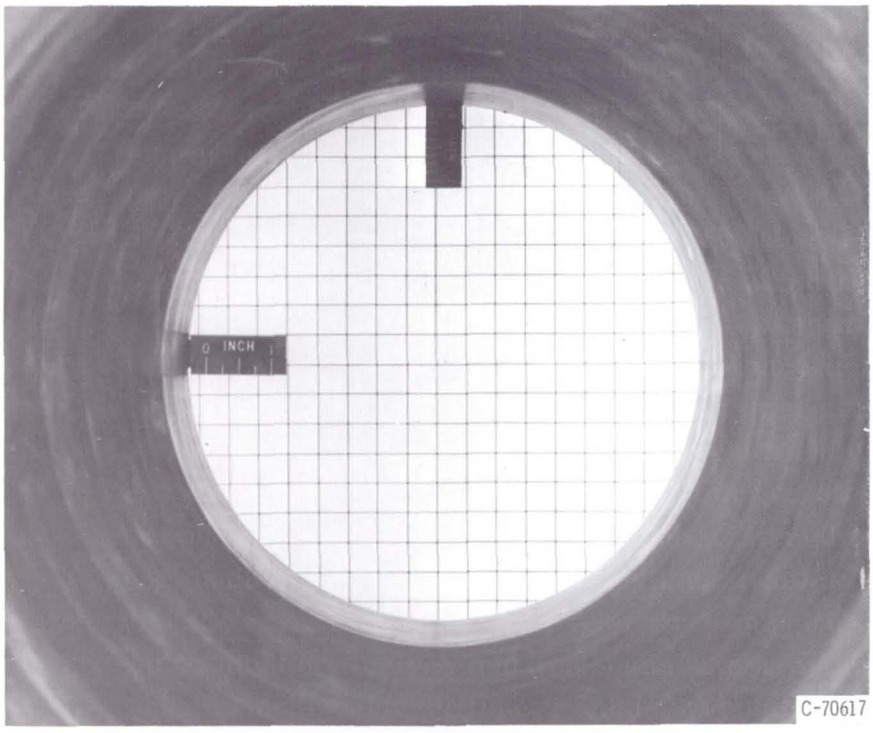

(a) Chamber 1, 0 seconds.

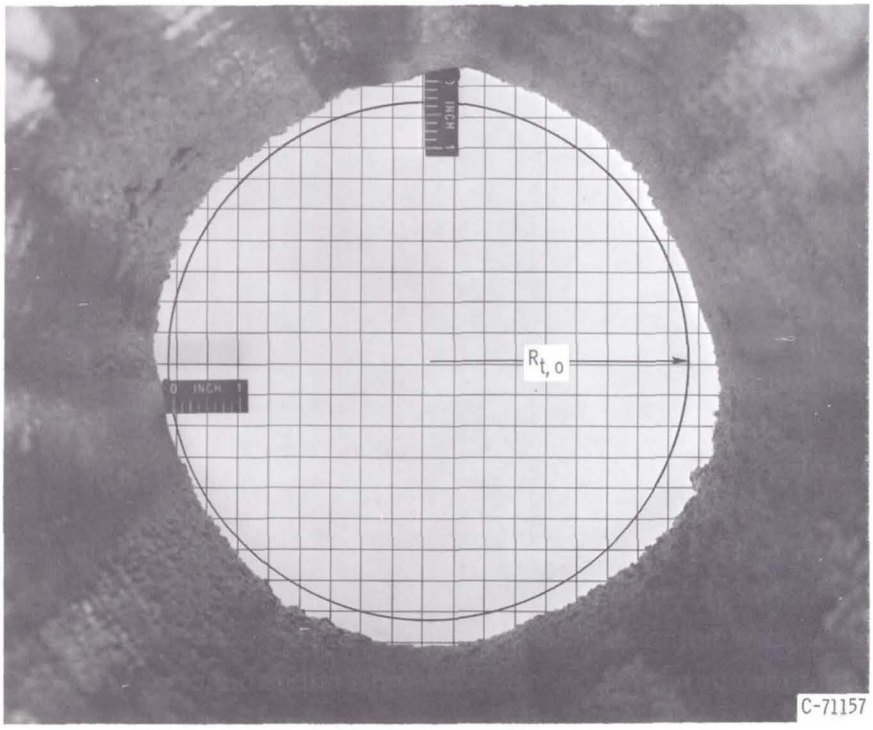

(b) Chamber 1, 679 seconds.

Figure 5. - Throat.

The equations of the flow equation procedure are given as follows:

Instantaneous throat area,

$$A_t(\theta) = \frac{(\eta_{c^*}, I^{c^*}_{th\text{-}eq})\dot{W}_t(\theta)}{gC_d(\varphi P_{c,i})} \tag{8}$$

Instantaneous effective throat-radius change,

$$\Delta R_t = \left[\sqrt{\frac{(\eta_{c^*}, I^{c^*}_{th\text{-}eq})\dot{W}_t(\theta)}{\pi g C_d(\varphi P_{c,i})}} - R_{t,o} \right] 10^3 \text{ mils} \tag{9}$$

where $R_{t,o}$ is the original throat radius.

RESULTS AND DISCUSSION

Combustion Conditions

In order that comparisons of ablative-material chambers be accomplished, all firings used the same propellant injector and were held at constant chamber pressure and oxidant-to-fuel ratio by the controller. Figures 6 and 7 present typical combustion conditions.

The variation of typical throat total chamber pressure with time is shown in figure 6(a). The steady-state chamber pressure of about 104 psia (717 kN/m^2) was obtained within 2 seconds from the signal to open the firing valves. A typical time history with oxidant-to-fuel ratio of 2.0 is shown in figure 6(b). The initial steady-state flow rates were about 20 pounds per second (9.08 kg/sec) of oxidant and 10 pounds per second (4.54 kg/sec) of fuel.

The combustion performance level is shown in figure 7 as determined from the vacuum specific impulse method. The c* efficiency was constant, over the range of oxidant-to-fuel ratios from 1.4 to 2.1, at about 98.3 percent for the duration of the investigation. Unpublished data acquired in another facility with the same engine are in excellent agreement with the data of the present investigation. Four time intervals of 1000 seconds each were selected to make the comparison of combustion performance level. The performance data taken in the first 3000 seconds were obtained with the 1.3-expansion-ratio nozzle (chamber of table III, configuration E).

There was no detectable performance deterioration despite the facts that the oxidant holes eroded and some holes were plugged, as noted earlier.

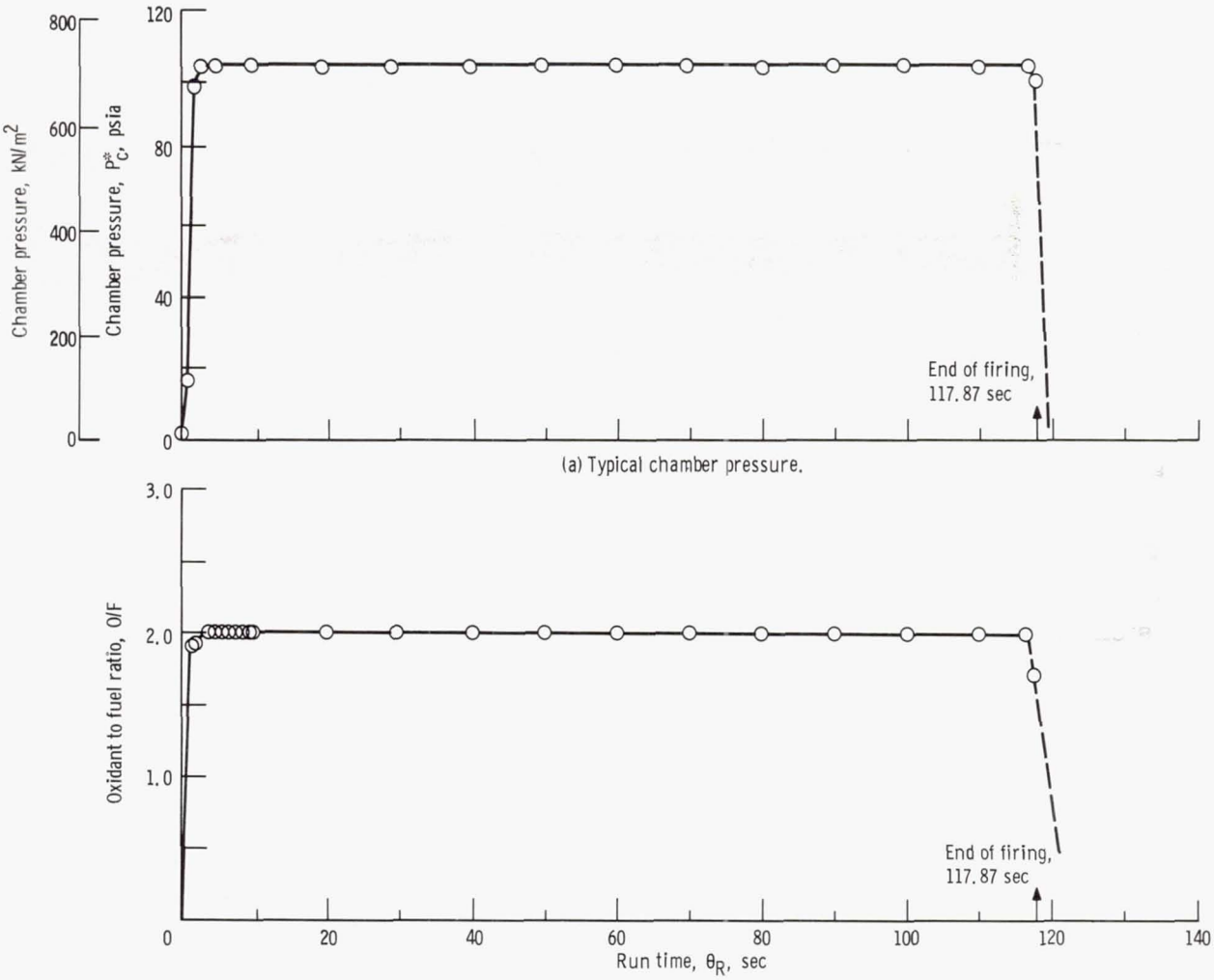

(a) Typical chamber pressure.

(b) Typical oxidant-to-fuel ratio.

Figure 6. - Combustion conditions. Accumulative firing time (3 firings) before this firing, 102.21 seconds.

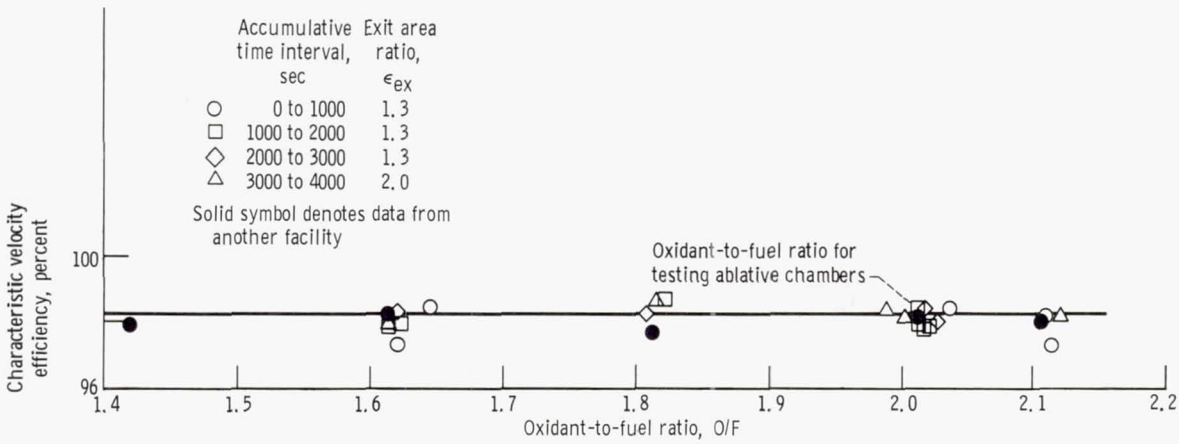

Figure 7. - Combustion performance.

TABLE IV. - ABLATIVE-CHAMBER TEST RESULTS

Chamber	Firing time, θ_R, sec	Accumulative firing time, θ_A, sec	Time average steady-state chamber pressure, P_c, psia (a)	Time average steady-state oxidant-to-fuel ratio, O/F	Throat area at end of firing, $A_t(\theta)$, $in.^2$ (b)	Overall linear erosion rate, mil/sec (c)
1	0	0	-----	----	48.27	----
	2.86	2.86	-----	----	-----	----
	5.96	8.82	106	2.02	47.98	----
	105.35	114.17	105.7	2.02	47.71	----
	110.42	224.59	105.6	2.01	48.66	0.09
	5.95	230.54	105.9	2.01	48.88	.10
	98.4	328.94	105.9	2.01	49.95	.20
	102.07	431.01	105.6	2.01	51.6	.30
	6.10	437.11	105.6	2.02	-----	----
	64.25	501.11	105.2	2.02	52.46	.34
	6.08	507.2	106.2	2.03	52.80	.36
	91.37	598.57	105.9	2.03	53.57	.35
	80.43	678.97	106	2.03	55.08	.39
	103.78	782.75	106.1	2.03	57.42	.45
	90.55	873.30	106.4	2.00	58.41	.46
	93.95	967.25	106.2	2.01	63.53	.59
2	0	0	-----	----	48.1	----
	2.63	2.63	-----	----	-----	----
	3.00	5.63	-----	----	-----	----
	5.00	10.63	106.0	2.02	48.03	----
	4.84	15.47	105.8	2.02	48.08	----
	99.54	115.01	102.6	2.03	47.21	----
	109.05	224.06	102.6	2.04	48.48	0.07
	5.05	229.11	106.7	2.02	48.61	.09
	5.06	234.17	105.0	2.02	48.75	.11
	78.22	312.39	105.6	2.02	49.35	.16
	105.30	417.69	105.7	2.02	52.03	.38
	90.63	507.17	106	2.02	59.13	.84
	83.64	591.96	106.8	2.05	66.30	1.15
3	0	0	-----	----	49.22	----
	2.13	2.13	-----	----	-----	----
	1.99	4.12	-----	----	-----	----
	5.1	9.19	100.6	2.03	49.26	----
	49.88	59.07	100.1	2.02	48.76	----
	70.75	129.82	100.3	2.02	51.16	0.60
	93.5	223.32	100.3	2.02	58.80	1.66
4	0	0	-----	----	48.09	----
	4.99	4.99	106.4	2.02	-----	----
	4.88	9.87	105.7	2.02	48.32	1.01
	98.96	108.83	105.7	2.04	49.80	.63
	80.60	189.43	105.9	2.04	53.33	1.11
	35.36	224.79	104.9	2.02	55.35	1.27
5	0	0	-----	----	48.20	----
	6.00	6.00	104.6	2.01	48.1	----
	34.31	40.31	104.9	2.00	47.26	----
	61.90	102.21	104.4	2.00	46.75	----
	117.88	220.09	104.6	2.00	46.82	----
	117.9	337.99	105.8	1.99	47.82	----
	111.09	449.08	103.7	2.07	51.04	0.26
	102.9	551.98	103.8	2.01	58.80	.92
	2.4	554.38	-----	----	-----	.92
6	0	0	-----	----	48.25	----
	5.95	5.95	104.7	1.99	48.24	----
	33.84	39.79	104.2	2.01	48.06	----
	62.1	101.89	103.4	1.98	47.46	----
	119.48	221.37	104.1	2.01	47.88	----
	112.79	334.16	103.8	1.99	54.50	0.73
	29.00	363.16	103.4	2.02	55.28	.74
	17.78	380.94	104.3	2.02	56.65	.86
	56.02	436.96	104.4	1.99	61.36	1.15
	7.14	444.10	-----	----	-----	----
	51.62	495.72	102.5	2.00	65.53	1.49

[a] Corrected to throat total pressure. To convert to kN/m^2 multiply by 6.895.

[b] To convert square inches to square meters, multiply by 6.4516×10^{-4}.

[c] To convert mil/sec to mm/sec multiply by 0.0254.

The erosion rate at the throat of ablative chambers is strongly influenced by the gas stream temperature, which is in turn influenced by characteristic velocity efficiency and oxidant-to-fuel ratio distribution. Characteristic velocity efficiency was relatively high, about 98.3 percent, for the present investigation. At an overall oxidant-to-fuel ratio of 2.0, the injector design provided a core region (the triplet elements) wherein nominally 85 percent of the total propellant flow was introduced at an average oxidant-to-fuel ratio of about 2.15; about 14.2 percent of the total flow was introduced by showerhead elements surrounding the triplet elements, at an average oxidant-to-fuel ratio of about 1.56. The downstream circumferential edge of the injector was film cooled by the introduction of 2.4 percent of the fuel (0.8 percent of total flow). Stratification of the oxidant-to-fuel ratio distribution provided by the injector design undoubtedly reduced the erosion rates to be discussed in the following sections.

Erosion of Full-Length Ablative Chambers

Table IV summarizes the test conditions and results for the ablative chambers. This table provides the chamber number, firing time, accumulative firing time, time average steady-state chamber pressure, oxidant-to-fuel ratio, the throat area at the end of each firing, and the overall erosion rate $\left\{\left[R_t(\theta) - R_{t,o}\right]/\theta\right\}$ in mils per second (0.0254 mm/sec) at the end of each firing.

Chamber 1. - The results for chamber 1 (silica-cloth - phenolic-resin material, with a 60° fiber-orientation angle throughout the length of the chamber) are presented in figure 8. Throat radius and percent area change as functions of accumulative firing time are presented in figure 8(a); post-firing photographs are shown in figures 8(b) and (c). The throat radius and percent area change obtained from the flow equation procedure are compared with measurements made by the micrometer and the photographic procedures (fig. 8(a)). The results for throat radius and percent area change for all the ablative chambers will be discussed primarily on the basis of the flow equation procedure. Values for throat radius change were calculated at 0.96-second intervals and are therefore presented as a continuous line. As indicated by these data, agreement between the procedures was excellent during the initial stages of testing. For the first 500 seconds, disagreement between procedures was less than 2 percent of area change. A total of fifteen major and minor firings were made on chamber 1. (See table IV.) The end of major rocket firings are indicated by vertical arrows (fig. 8(a)).

Lines of constant overall erosion rate have been added as an aid in determining instantaneous values of overall erosion rate along the curve. The minimum point of the curve (fig. 8(a)) at 50 seconds is probably the result of thermal expansion, silica-melt flow, an increase in weight flow from phenolic vaporization, and a boundary-layer-

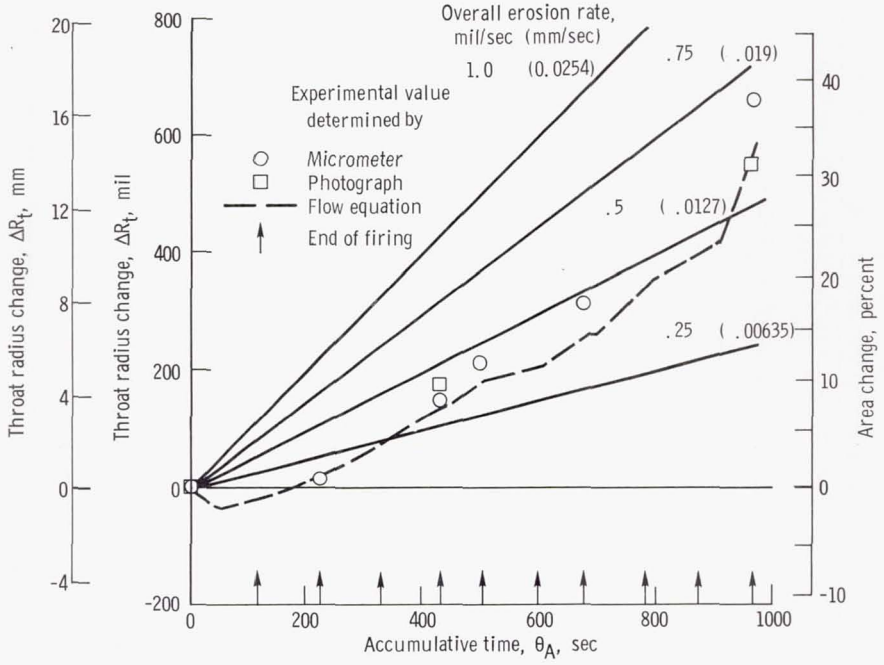

(a) Dimensional time.

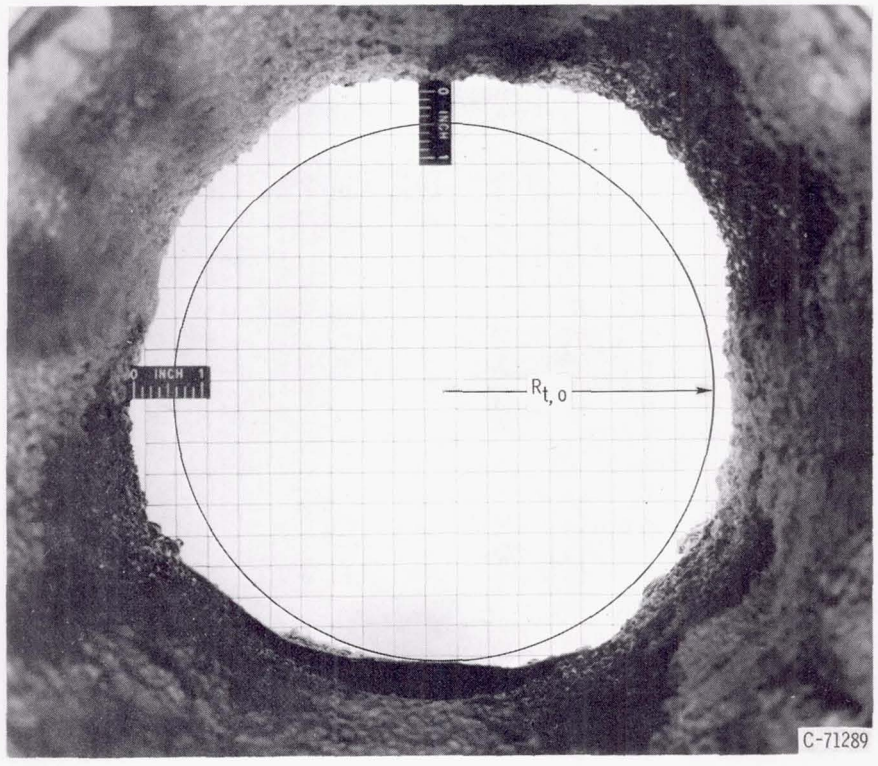

(b) Chamber throat after 967 seconds. Circle is original throat diameter of 7.82 inches.

Figure 8. - Chamber 1; silica-cloth - phenolic-resin material; fiber-orientation angle, 60° throughout.

(c) Cross section of chamber after 967 seconds.

Figure 8. - Concluded.

thickness increase resulting from phenolic vaporization. For chamber 1 at about 60 seconds of total firing time, there was about a 30-mil (0.762 mm) reduction in radius or approximately a 1.5-percent reduction in throat area. The crossover point, after which the start of positive values of ΔR_t exist, occurred after 170 seconds of firing time. The overall erosion rate at an accumulative time of 910 seconds was 0.45 mils per second (0.0114 mm/sec), and the throat had undergone a 24-percent increase in area. An overall erosion rate of 0.5 mils per second (0.0127 mm/sec) for an accumulative time of about 750 seconds was considered a reasonable value for the conditions of the present investigation. These values of overall erosion rate would be acceptable on engines larger than those tested in this investigation, but might be considered excessive on smaller engines (e.g., ref. 1 to 3) where the percent change in area ratio is greater for a given value of overall erosion rate. A pronounced increase in the slope of the curve occurred after 910 seconds, suggesting the possibility of charring through to the fiber-glass wrap (fig. 8(c)), a depletion of ablation gases, and therefore a nominal engine failure. Chamber 1 was tested for a total accumulative time of 967 seconds. The final overall erosion rate was 0.59 mils per second (0.015 mm/sec), and the throat had undergone a 34-percent increase in area. Positions along the curve where little or no change of throat radius occurred were thought to have resulted from a warmup period which occurred at the start of each firing.

The final throat-area photograph for chamber 1 is shown in figure 8(b). Gouging of the chamber was present but not extreme. The gouges were probably the results of spurious injector oxidant jets which had developed as a result of erosion around injector holes.

The chamber developed a very thick, tenacious, uniform char over its length, which can be seen in the photograph of figure 8(c). The char thickness was more than 1000 mils (25.4 mm). Little or no erosion occurred in the chamber section. Cracking and separation between the inner layer and the outer flat wrap layer appeared to be minor.

Chamber 2. - The results for chamber 2 (silica-cloth - phenolic-resin material, with a 60° fiber-orientation angle in the chamber and molded 1/2-inch-square (1.27 cm) material in the throat region) are presented in figure 9. Agreement between the three methods of obtaining throat-radius change was excellent over most of the time history as can be seen in figure 9(a). A total of six major and six minor firings were made on chamber 2 (table IV).

The minimum point of the curve indicates about a 40-mil (1.014 mm) reduction in throat radius, or approximately a 2-percent area decrease, and occurred at about 90 seconds of accumulative firing time. The crossover point occurred at about 210 seconds of accumulative firing time. A pronounced increase in the slope of the curve of throat-radius change occurred after 380 seconds of accumulative firing time. This increase suggests that charring beyond the inner layer had occurred. At 380 seconds, the chamber

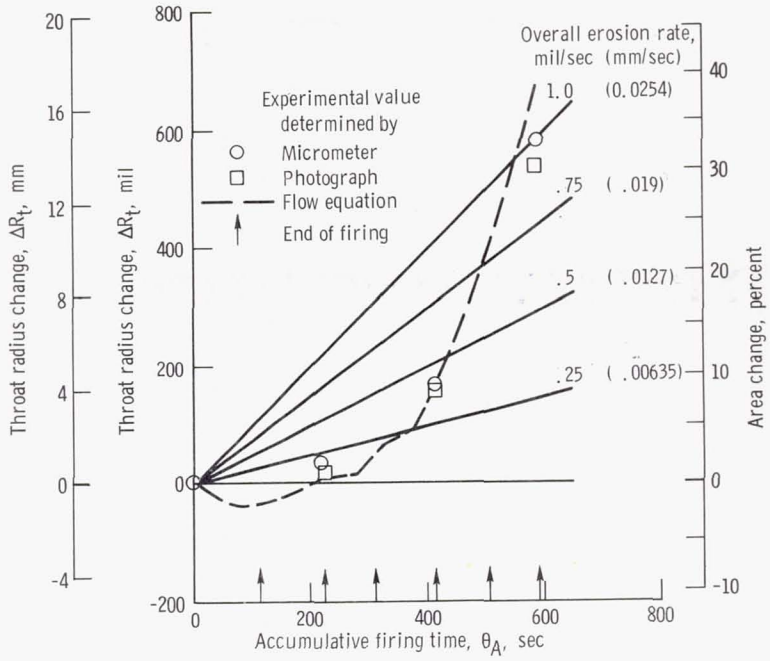

(a) Dimensional time.

(b) Magnified cross section of molded 1/2-inch squares of material.

Figure 9. - Chamber 2; silica-cloth - phenolic-resin material; fiber-orientation angle, 60° in the chamber and 1/2-inch squares in the throat.

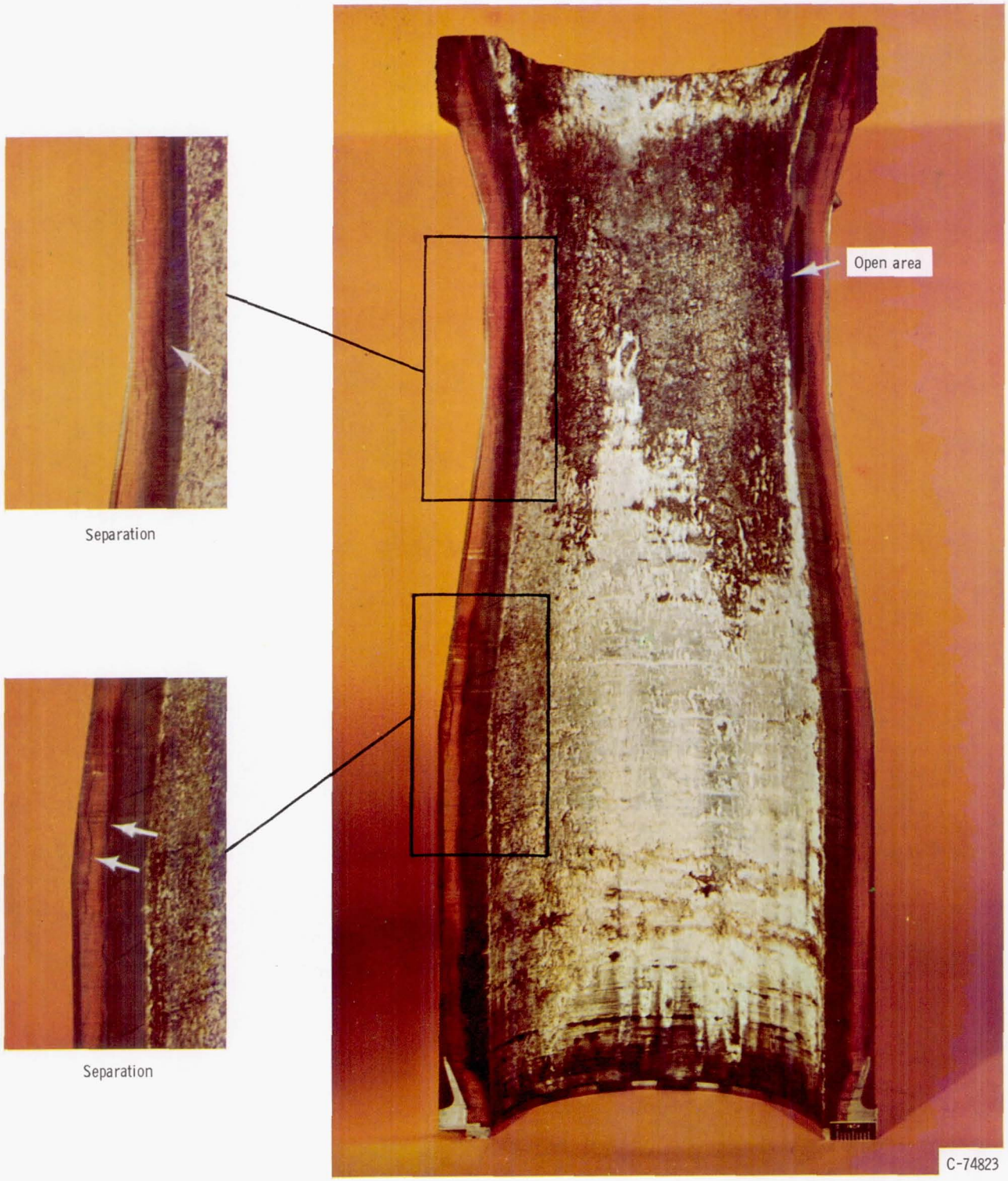

(c) Cross section of chamber after 592 seconds.

Figure 9. - Concluded.

had undergone a 100-mil (2.54 mm) throat-radius change or a 5-percent increase in throat area, and the overall erosion rate was 0.26 mil per second (0.0066 mm/sec). The overall erosion rate was less than 0.5 mil per second (0.0127 mm/sec) for the first 430 seconds of accumulative firing time. Chamber 2 was tested for a total accumulative firing time of 592 seconds at which time the overall erosion rate was about 1.15 mils per second (0.0258 mm/sec), or about a 38-percent increase in throat area had occurred. Thus, between 380 and 592 seconds of accumulative firing time, approximately a 30-percent increase in throat area had occurred, which is considered excessive erosion.

A photograph of the cross-sectioned molded 1/2-inch-square (1.27 cm) material used in the throat region is shown in figure 9(b) magnified several times.

Chamber 2 developed a very thick, tenacious char layer, which was about 1000 mils (25.4 mm) thick in the chamber and 750 mils (19 mm) thick in the throat. Thus, charring had penetrated into the outer flat wrap layer as shown in figure 9(c). Little or no erosion occurred in the chamber section, and streaking and gouging were minimal in both the chamber and the throat regions. Separation of the inner layer from the outer flat wrap layer did occur but did not impair the structural integrity of the chamber for the testing duration as indicated in the photograph of figure 9(c). The open area (on the right side of the chamber-throat photograph) resulted when the chamber was cross sectioned.

Chamber 3. - The results for chamber 3 (silica-cloth - phenolic-resin material with 13-percent elastomer additive to the total weight of inner ablative layer and a 60° fiber-orientation angle throughout the length of the chamber) are shown in figure 10. Good agreement was obtained between the three methods of determining the throat radius and percent area change as may be seen from the results of figure 10(a). Three major and three minor firings were made on chamber 3 (table IV).

The minimum point of the throat-radius-change curve indicated about a 20-mil (0.508 mm) reduction in throat radius, or approximately a 1-percent reduction in throat area, and occurred at about 50 to 60 seconds of accumulative firing time. The crossover point occurred at about 80 seconds. Following the first 50 seconds of accumulative firing time, chamber 3 was left in the test stand for 60 hours with a propellant pool standing in the chamber; this was done unintentionally and was the result of improper flushing of the injector and the propellant lines as part of the engine shutdown procedure.

After the next major firing (130 sec of accumulative firing time), separation of the inner layer from the outer flat wrap layer was experienced; the overall erosion rate at this point was 0.58 mils per second (0.0147 mm/sec). The aforementioned separation of the layers could have contributed to the shift and change of slope of the subsequent throat-radius-change curve. Extrapolation of the curve from before 130 seconds on to 225 seconds of accumulative time indicates that possibily the overall erosion rate at 225 seconds could have been 1 mil per second (0.0254 mm/sec) had the chamber not been damaged. Chamber 3 was tested for a total time of 223.3 seconds, at which time the throat had

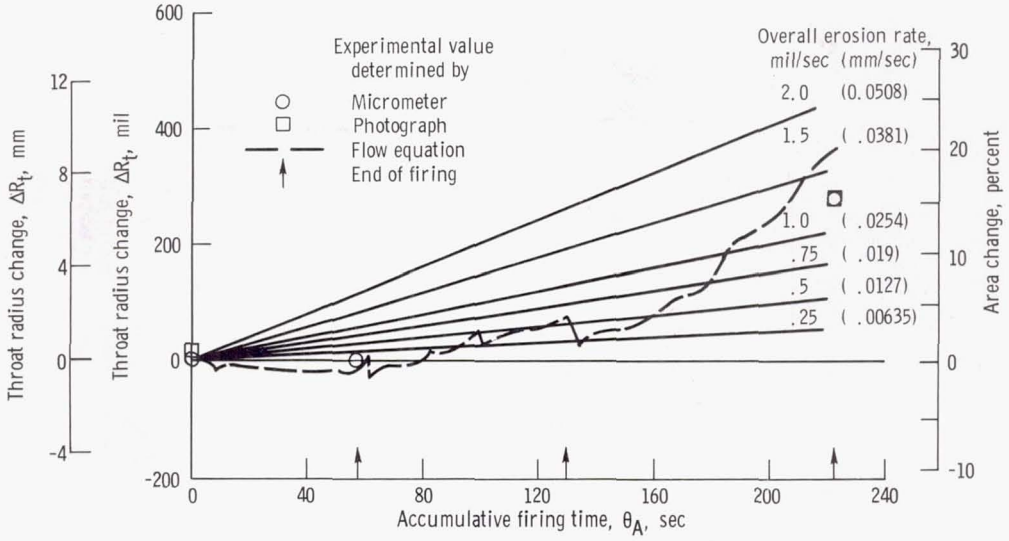

(a) Dimensional time.

(b) Cross section of chamber after 223 seconds.

Figure 10. - Chamber 3; silica-cloth - phenolic-resin material with elastomer additive; fiber-orientation angle, 60° throughout.

(c) Chunkout regions in the chamber section after 223 seconds.

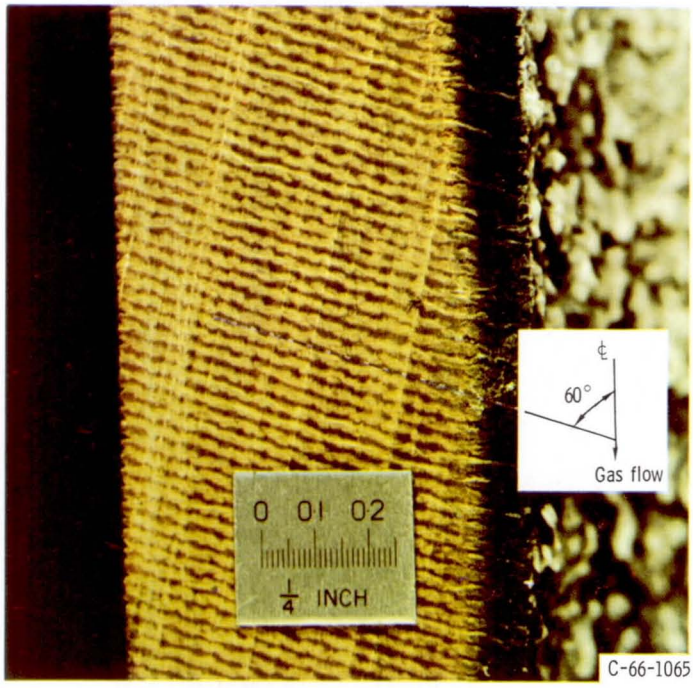

(d) Magnified cross section of typical silica-cloth - phenolic-resin material with elastomer additive; fiber-orientation angle, 60° to centerline.

Figure 10. - Concluded.

undergone a 370-mil (9.4 mm) increase (a 20-percent area increase), and the overall erosion rate was about 1.66 mils per second (0.0422 mm/sec).

Chamber 3, unlike chambers 1 and 2, experienced extreme separation of the inner layer from the outer flat wrap layer as is visible in figure 10(b). Separations in the throat region could be as much as 300 mils (7.62 mm). Figures 10(b) and (c) are post-firing photographs of chamber 3, and the large chunk-out regions that were produced during the last firing are visible. The chunk-out region at the bottom of the chamber was believed to be the result of the propellant soaking into the ablative material after the first major firing. The char thickness varied from about 750 mils (19 mm) in the chamber to about 500 mils (12.7 mm) in the throat region. Little or no erosion occurred in the chamber section; streaking and gouging were slight, if the chunk-out regions are disregarded. Very little can be concluded regarding the effect of the elastomer additive on erosion because of the possible effect of propellant soaking.

A photograph of the cross-sectioned material of chamber 3 with a fiber-orientation angle of 60° is shown in figure 10(d) magnified several times.

Chamber 4. - The results for chamber 4 (graphite-cloth - phenolic resin material, with a 60° fiber-orientation angle) are shown in figure 11. In general, good agreement was obtained among the three methods of obtaining throat radius and percent area change as shown in figure 11(a). A total of three major and two minor firings was made on chamber 4 (table IV). A decrease in throat area was not observed for chamber 4; therefore, there was no crossover point. The apparent reasons for this are the absence of melted material flowing from upstream of the throat and little or no thermal-chemical expansion of the ablative material. These results indicate that the negative area for the other chambers may not be due to gases injected causing boundary-layer thickening as previously hypothesized. An overall erosion rate of 0.5 mil per second (0.0127 mm/sec) occurred within 75 to 80 seconds. This time is significant in that chamber 3 required 130 seconds to reach 0.5 mil per second of overall erosion rate and therefore would tend to indicate that chamber 4 was less resistant to erosion than chamber 3. Reference 3 indicated the erosion of graphite-cloth material was probably due primarily to oxidation. The overall erosion rate at 225 seconds of accumulative time was 1.27 mils per second (0.0323 mm/sec) (table IV and fig. 11(a)), which was equivalent to a throat-area increase of 15 percent at the termination of testing on chamber 4.

The post-firing photograph of figure 11(b) indicates that approximately a 50-mil (1.27 mm) separation of the inner layer from the outer flat wrap layer occurred in the throat region. Figure 11(b) indicates that little or no erosion occurred in the chamber section and that streaking and gouging were minimal. Testing of chamber 4 was terminated because of charring to the outside and failure at the flange connecting the chamber to the injector. The graphite-cloth material of chamber 4 develops a char at a much faster rate than the silica-cloth materials. This char is due to the high thermal conduc-

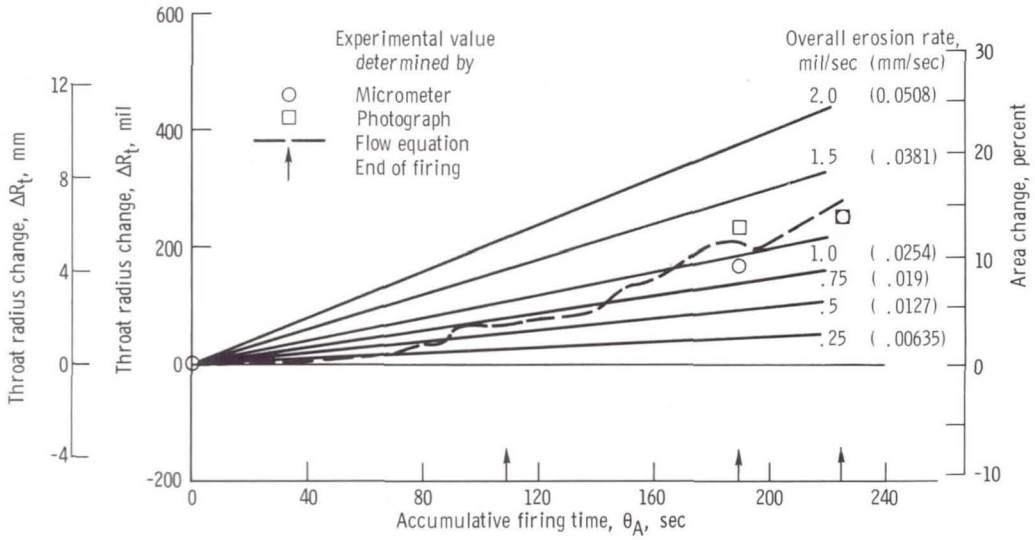

(a) Dimensional time.

(b) Cross section of chamber after 225 seconds.

Figure 11. - Chamber 4; graphite-cloth - phenolic-resin material; fiber-orientation angle, 60° throughout.

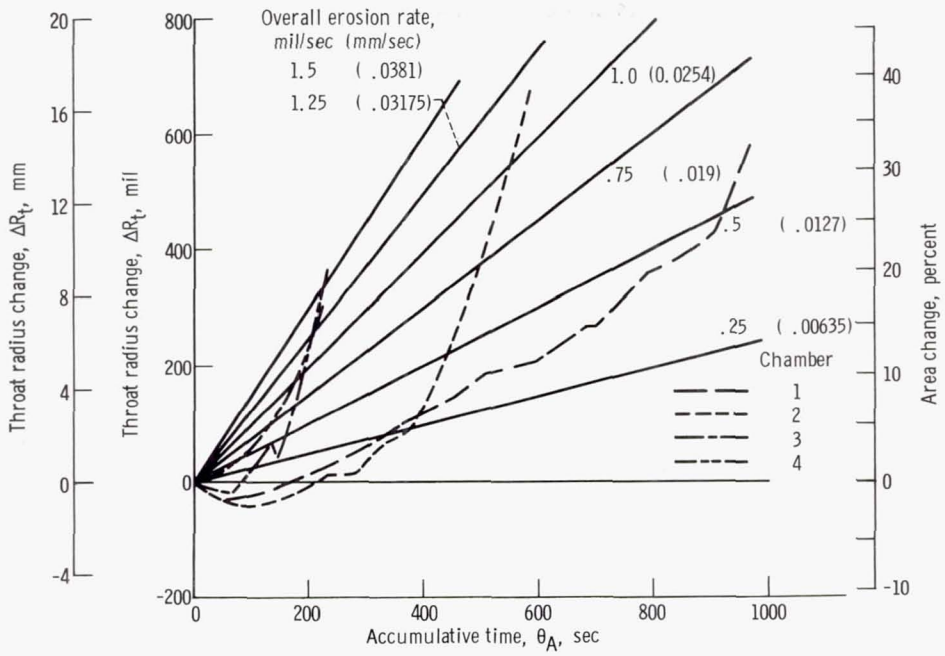

Figure 12. - Comparison of erosion of four ablative materials.

tivity (ref. 1) of the graphite cloth.

Comparison of chambers 1 to 4. - The results of testing the full-length ablative chambers are summarized in figure 12, where a comparison is made of the throat erosion of the four materials. For chambers 1 and 2, the trend of the throat-radius-change curves is virtually the same through the first 400 seconds of accumulative firing time. The trend after 400 seconds, however, indicates that the preferentially oriented fiber material (with a 60° angle) of chamber 1 is superior to the molded 1/2-inch-square (1.27 cm) fibers of chamber 2 when compared on the basis of erosive resistance.

Comparing the throat erosion of chamber 3 to that of chambers 1 and 2 indicates that a 13 percent by weight additive of an elastomer to the phenolic resin did not inhibit erosion but, in fact, increased erosion. The results for chamber 3, however, may be affected by the propellant soaking into the chamber.

The data of figure 12 indicate that the graphite-cloth - phenolic-resin material of chamber 4 has inferior erosion resistance when compared to that of the silica-cloth - phenolic-resin materials of chambers 1 and 2. The first three chambers of figure 12 have throat-radius-change curves which have minimum points and, therefore, crossover points, which is not the case with chamber 4. It must, therefore, be concluded that thermal-chemical expansion of material is the least on chamber 4, that oxidation of the material is high, and/or that the sum of upstream melted and gaseous material is at a minimum for chamber 4 as compared to chambers 1 to 3.

Erosion of Short Ablative Chambers

Chambers 5 and 6 were short ablative chambers, which were tested with a water-cooled cylindrical section upstream in order to give nearly the same overall characteristic length as the full-length ablative chambers. There was more than 12 inches (30.48 cm) less ablative material upstream of the throat than on chamber 1 (cf. table III, configurations A and B). Also the ablative inner layer was 1.5 inches (38.1 mm) thick, and there was no outer flat wrap layer. Chamber 5 was of a tubular throat design and chamber 6 of a contoured throat design as indicated by tables I and III.

Chamber 5. - Figure 13 presents the results for chamber 5 (silica-cloth - phenolic-resin material with a fiber-orientation angle of 60° throughout). Comparing the procedures of determining the throat-radius change indicates excellent agreement between the micrometer, the photograph, and the flow equation. A total of six major and two minor firings was made on chamber 5 (table IV). The minimum point of the throat-radius-change curve indicated about a 50-mil (1.27 mm) reduction in throat radius and occurred at about 150 seconds of accumulative time. The crossover point did not occur until 410 seconds, after which a rather rapid erosion occurred. The crossover point for chamber 5 occurred 240 seconds later than that of chamber 1, which was full length. The results with chamber 1 could have been influenced by injector hole edge deterioration leading to poor impingement of some elements and subsequent gouging. A suitable injector-repair procedure was just being established at this time. No conclusive explanation, however, can be given for the crossover point occurring after such a large time with chamber 5. Erosion to an overall erosion rate of 0.5 mil per second (0.0127 mm/sec) occurred at 490 seconds of accumulative time. Chamber 5 was tested for a total accumulative time of 554 seconds at which time an overall throat-radius change of about 520 mils (13.17 mm) (a 29-percent throat-area increase) had occurred, and the overall erosion rate was about 0.92 mil per second (0.0233 mm/sec).

The post-firing photograph of figure 13(b) indicates that the char thickness in the throat region was about 600 mils (15.2 mm) (after 554 sec), which is about the same as the throat-radius change at this time. The char thickness is about 700 mils (17.8 mm) in the chamber region of chamber 5, which is about 300 mils (7.62 mm) less than that obtained on chamber 2; chambers 2 (a full-length ablative chamber) and 5 were tested for about the same total duration of 550 seconds. The photograph indicates that about 250 mils (6.35 mm) had eroded away in the chamber region. Streaking and gouging were minimal throughout the chamber.

Chamber 6. - The results for chamber 6 are presented in figure 14. Chamber 6 was identical to chamber 5 except that chamber 6 had a contoured throat instead of a turbular throat. The three procedures of obtaining throat-radius change are in good agreement over the entire duration of testing. Table IV indicates a total of eight major and two

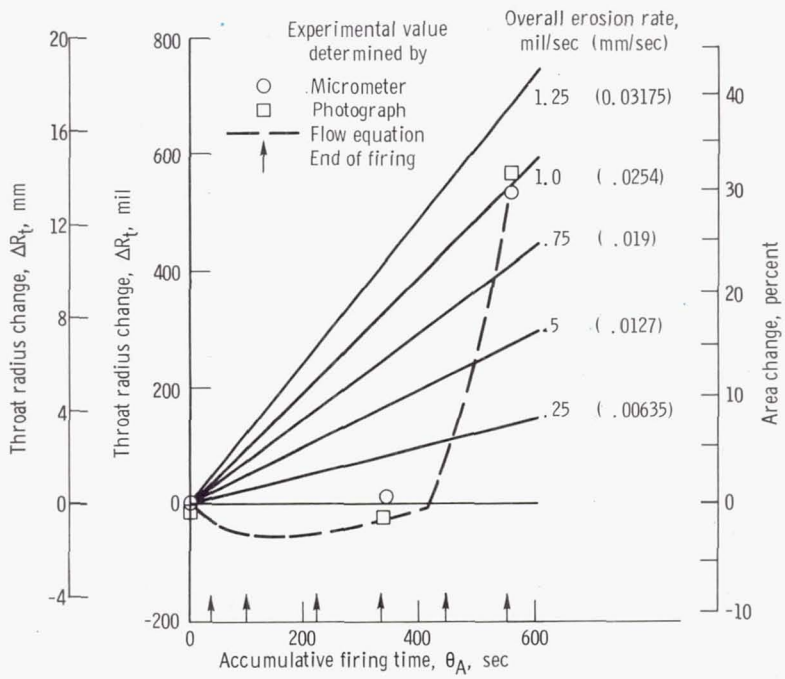

(a) Dimensional time.

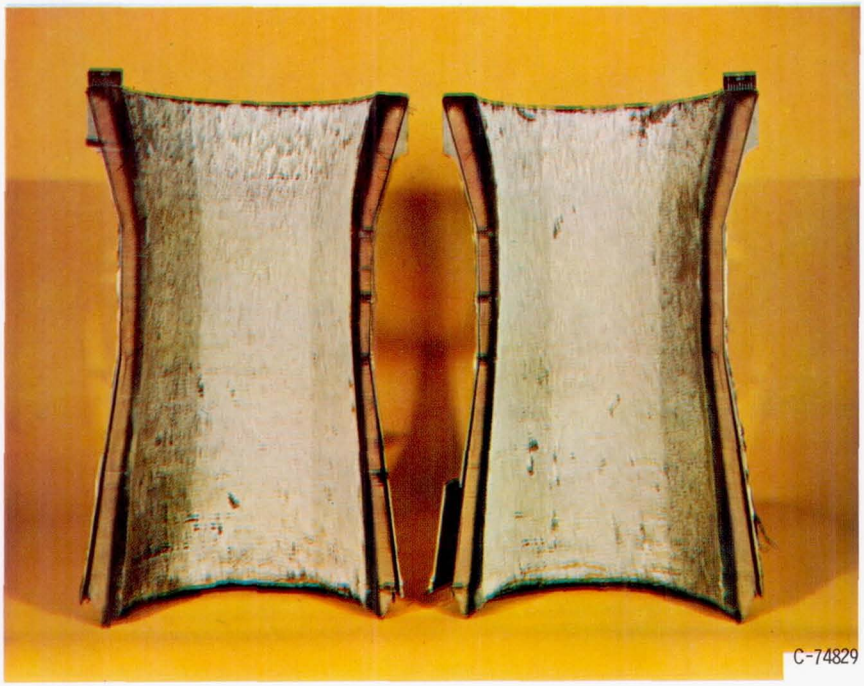

(b) Cross section of chamber after 554 seconds.

Figure 13. - Chamber 5; silica-cloth - phenolic-resin material; fiber-orientation angle, 60° throughout.

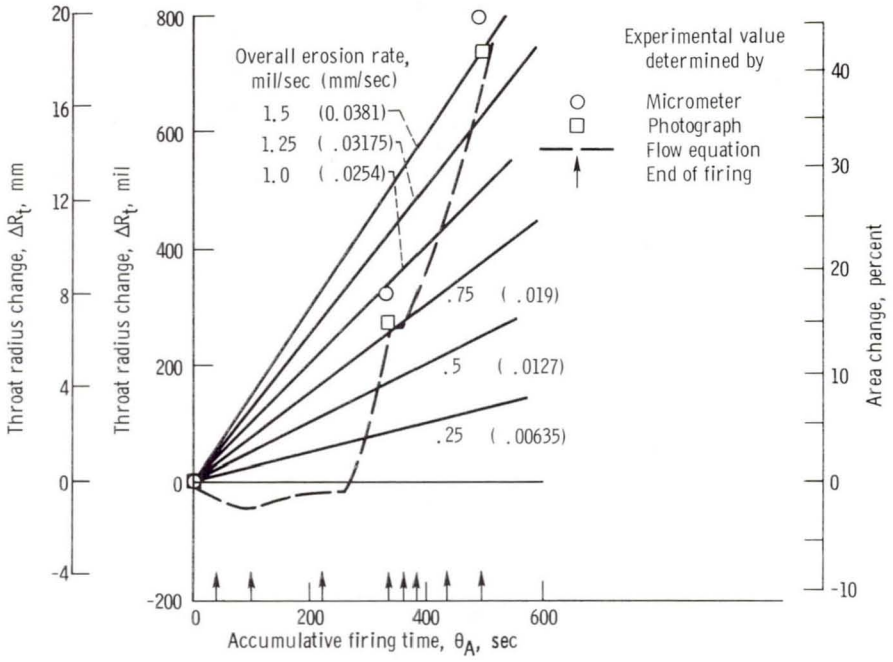

(a) Dimensional time.

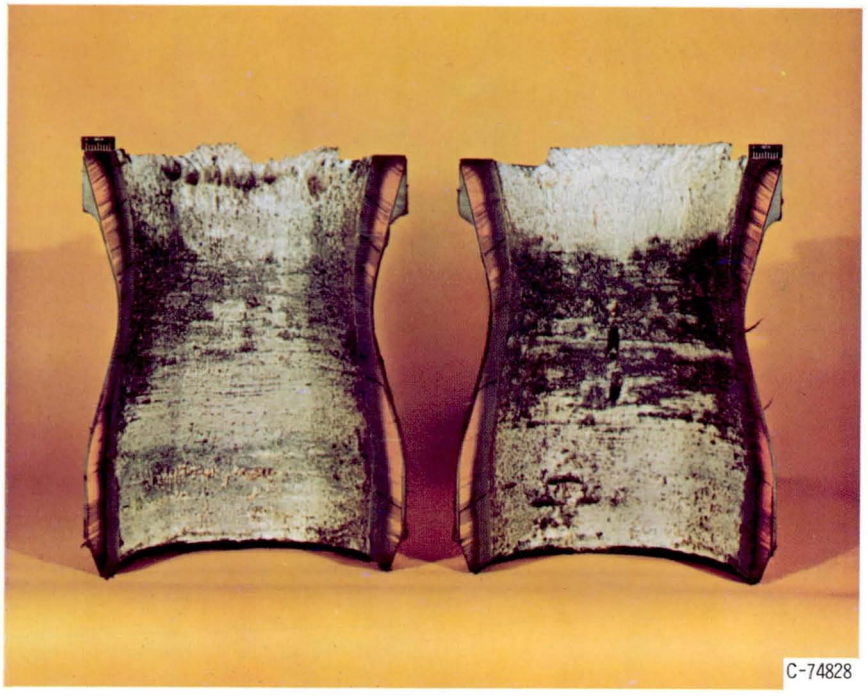

(b) Cross section of chamber after 496 seconds.

Figure 14. - Chamber 6; silica-cloth - phenolic-fiber material; fiber orientation angle, 60° throughout.

minor firings was made on chamber 6. The minimum point of the throat-radius-change curve indicated about a 45-mil (1.14 mm) reduction in throat radius and occurred at about 90 seconds. The crossover point occurred at 276 seconds of accumulative time, after which a rather rapid erosion occurred. Erosion to an overall erosion rate of 0.5 mil per second (0.0127 mm/sec) occurred at 315 seconds. Chamber 6 was tested for a total accumulative time of 496 seconds, and the throat-radius change was 740 mils (18.8 mm) (a 43-percent throat-area increase) yielding an overall erosion rate of 1.49 mils per second (0.0379 mm/sec).

The char thickness was about 750 mils (19 mm) in the throat region as indicated in figure 14(b). This thickness was similar to the char-layer thickness and final throat-radius change of chamber 5. Figure 14(b) also indicates that about 500 mils (12.7 mm) of ablative material had eroded away in the chamber section.

Comparison of chamber geometry effects. - Figure 15 summarizes the effects of modifications to ablative-chamber geometry on throat erosion, for chambers of the same material. Chamber 1, which was of ablative material for its full length, had the best throat-erosion resistance for durations over 470 seconds indicating a beneficial effect of the materials evolving from the upstream region, perhaps in the form of a gaseous insulating layer along the surface. The apparent reason for chamber 1 not having the best throat erosion before 470 seconds is the fact that the injector deteriorated during the earlier stages of testing. The injector deterioration was in the form of spurious oxidant jets, which impinged on the walls of the ablative chamber, and is associated with chamber gouging. Chambers 5 and 6, which included water-cooled sections and, therefore,

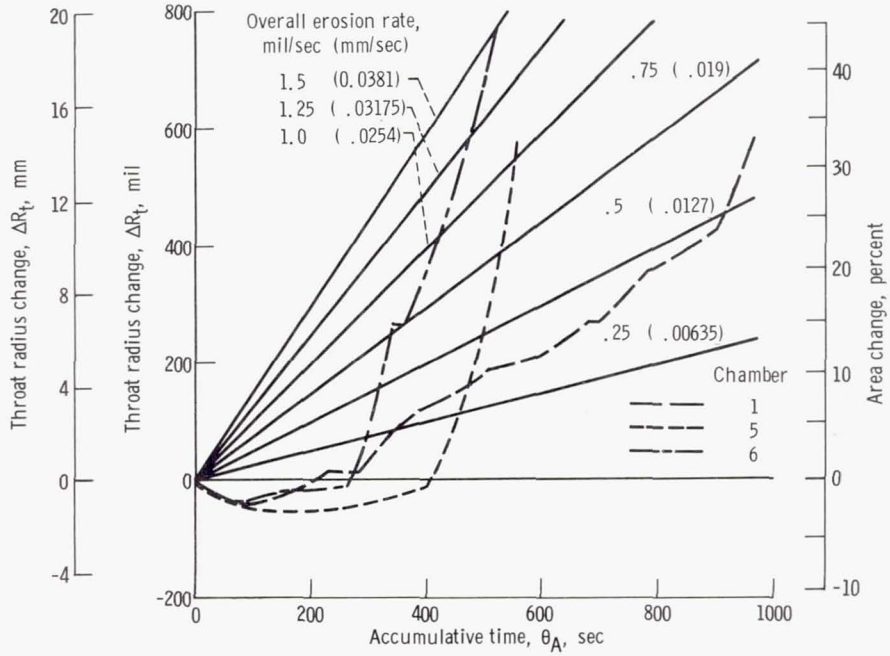

Figure 15. - Comparative effects of chamber geometry.

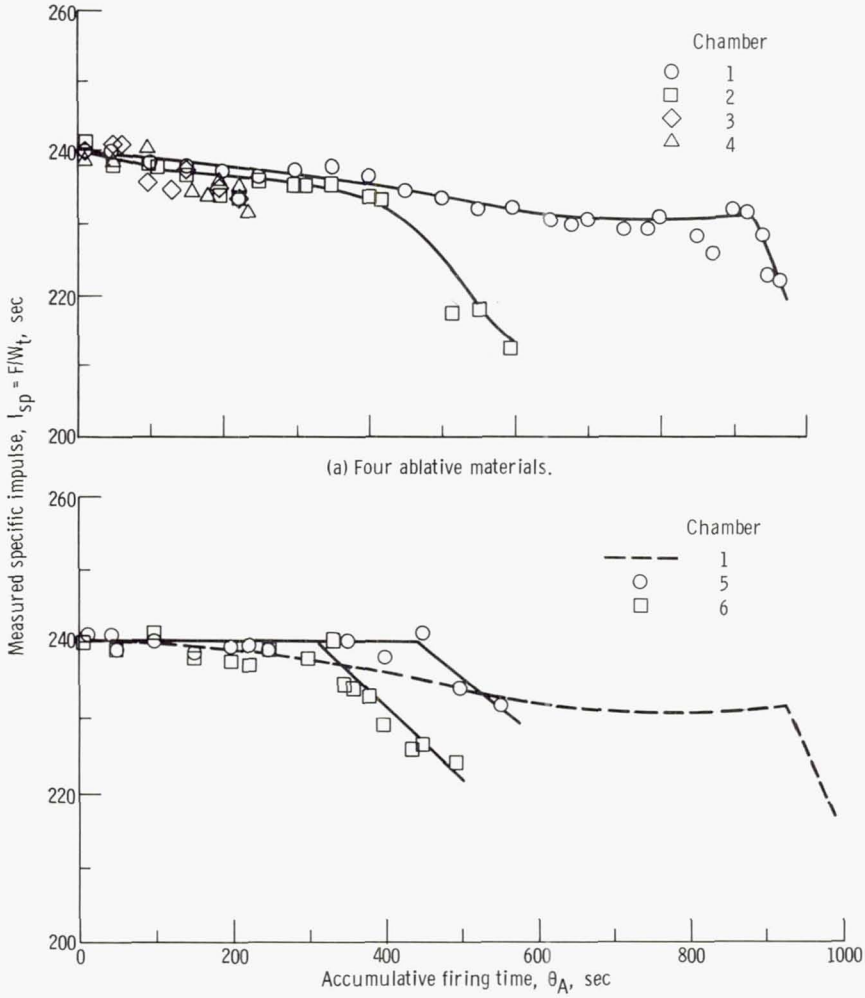

(b) Geometry.

Figure 16. - Specific-impulse decay resulting from throat erosion.

less ablative material ahead of the throat, had poorer throat-erosion resistance. Chamber 1 permitted about 400 seconds greater firing time than chamber 5 for a 30-percent increase in throat area.

Comparing the two short chambers, chambers 5 and 6, and the data of figure 15 indicates that the maximum negative throat-radius change of the short contoured-throat ablative chamber was 5 mils (0.127 mm) less than that of the short tubular-throat ablative chamber and occurred 60 seconds earlier. The crossover point for chamber 6 occurred at 276 seconds, which was 134 seconds earlier than that of chamber 5. The tubular throat appears to delay the onset of an increasing throat-radius change by way of the time required to erode a tubular throat into a contoured throat. Increasing the throat length to 0.77 times its diameter increased the chamber life by more than 150 seconds for area changes up to 13 percent and diminished to slightly under 100 seconds thereafter. The increased throat length increased engine weight by about 4.0 percent.

Specific Impulse

Measured specific impulse is presented as a function of accumulative firing time in figure 16 for the various ablative chambers. The specific-impulse decay, due to throat erosion, was generally gradual until a rapid increase in throat area occurred. A throat-area change of 30 percent resulted in an impulse decay of about 8.3 percent. The decay in measured specific impulse resulted from a decrease in area ratio from a value of 2.0 to about 1.5 (with an assumed constant exit area). The equivalent decay in specific impulse for a large-area-ratio nozzle ($\epsilon_{ex} \approx 60{:}1$) would be approximately 1 percent.

SUMMARY OF RESULTS

A series of six ablative-material thrust chambers with initial throat diameter of nominally 7.82 inches (19.8 cm) was evaluated as components of storable-propellant rocket engines. The propellants were nitrogen tetroxide N_2O_4 and a 50-50 blend of unsymmetrical dimethyl hydrazine with hydrazine N_2H_4. Engine operating conditions were maintained essentially constant by using the same propellant injector throughout the test series and an automatic controller to hold chamber pressure and oxidant-to-fuel ratio nominally at 100 psia (689 kN/m^2) and 2.0, respectively. Characteristic velocity efficiency was nominally 98 percent. The test series was conducted in an altitude facility at an ambient pressure of about 1.74 psia (12 kN/m^2). Four of the ablative-material thrust chambers provided materials variables, whereas two provided chamber-geometry variables. The results are as follows:

1. An ablative material of high-silica-cloth reinforcement and phenolic resin, with the reinforcement fibers oriented 60° downstream relative to the engine centerline, had the least throat erosion of the materials tested.

2. Molded 1/2-inch-square (1.27 cm) fiber reinforcement in the throat region of an ablative material, otherwise similar to that of result 1, increased the throat erosion.

3. An elastomer additive to an ablative material, otherwise similar to that of result 1, increased the throat erosion.

4. Graphite-cloth reinforcement, as compared to the high silica-cloth reinforcement of result 1, increased throat erosion.

5. An ablative-material chamber section with a 7.66° half-angle of contraction and a tubular throat (L/D = 0.77) provided about 100 seconds greater engine life, for the same percentage area increase, than did a chamber section of similar material with a 15° half-angle of contraction and a contoured throat.

6. A full-length ablative-material chamber had less throat erosion for run durations greater than 470 seconds than a chamber of essentially equal overall length but including a water-cooled section ahead of the ablative-material chamber section. The latter configuration exhibited a negative area change for the first 410 seconds.

Lewis Research Center,
National Aeronautics and Space Administration,
Cleveland, Ohio, November 10, 1966,
128-31-03-01-22.

APPENDIX A

SYMBOLS

A	geometrical area, sq in.
C_d	flow coefficient, actual flowrate/ isentropic one-dimensional flowrate
C_F	thrust coefficient, $F/P_c^*A_t$
c*	characteristic velocity, ft/sec (m/sec)
D	diameter, in. (m)
F	thrust, lb (N)
g	gravitational conversion factor, 32.174 ft/sec^2 (9.80665 m/sec^2)
I	specific inpulse, sec
L	length, in. (m)
L*	characteristic chamber length, chamber volume/throat area, in. (m)
P_c	chamber pressure, psia (N/m^2)
P_c^*	nozzle-throat-inlet total pressure, psia (N/m^2)
p	static pressure, psia (N/m^2)
p_o	altitude chamber pressure, static, psia (N/m^2)
R	radius, in. (m)
R_t	nozzle-throat radius, mil (mm)
t	thickness, in. (mm)
$\dot{W}$	propellant weight flow, lb/sec (kg/sec)
α	nozzle divergence angle, deg
β	nozzle convergence angle, deg
ϵ	area ratio (contraction or expansion)
η_{c^*}	characteristic velocity efficiency
η_{C_F}	thrust coefficient efficiency
$\eta_{I_{sp}}$	specific-impulse efficiency
θ	time, sec
λ	nozzle divergence correction, $1/2\ (1 + \cos \alpha)$
φ	momentum pressure loss

Subscripts:

A	accumulative
a	ablative
c	combustion chamber
cy	cylindrical
d	design
eq	equilibrium flow condition
ex	exit
f	fuel
fg	fiber-glass
i	injector
id	ideal conditions
m	measured
o	original or zero time, ambient, and oxidant
R	run
r	real
t	total

tc	contoured throat	w	water-cooled section
th	theoretical	v	vacuum conditions
tt	tubular throat	x	experimental

Conversion factors for International system of units:

To convert from U. S. customary unit	To International system of units	Multiply by
ft/sec^2	m/sec^2	$3.048\ (10^{-1})$
$in.^2$	m^2	$6.4516\ (10^{-4})$
gal	m^3	$3.785411784\ (10^{-3})$
lb-mass/sec	kg/sec	$4.5359237\ (10^{-1})$
lb-force	N	4.4482216152605
in.	m	$2.54\ (10^{-2})$
ft.	m	$3.048006096\ (10^{-1})$
mil	m	$2.54\ (10^{-5})$
lb-mass	kg	$4.5359237\ (10^{-1})$
$lb\text{-}force/in.^2$ (psi)	N/m^2	$6.8947572\ (10^3)$
sec	sec	1.00
ft/sec	m/sec	$3.048\ (10^{-1})$
deg	rad	$1.7453292519943\ (10^{-2})$

APPENDIX B

CALCULATION OF THRUST COEFFICIENT EFFICIENCY

The method for determining the thrust coefficient efficiency (for low-expansion-ratio nozzles) consisted of utilizing the theoretical divergence correction $1/2\ (1 + \cos \alpha)$, the theoretical thrust coefficients for one-dimensional equilibrium flow, the nozzle-pressure ratio, and the flow coefficient.

The analysis for obtaining the thrust coefficient efficiency was as follows: The thrust of a nozzle based on one-dimensional flow of an ideal gas is given by

$$F_{id} = \left(\frac{\dot{W}_{t,\,id}}{g}\right) V_{ex} + (p_{ex} - p_o) A_{ex} \tag{B1}$$

A similar analysis can be found in references 11 and 12.

For an axisymmetric real nozzle, a flow coefficient was used to account for three-dimensional effects and the influence of the nozzle wall at the throat producing nonuniform flow conditions in the throat region.

The divergence correction $\lambda = 0.983$ for a 15° half-angle conical nozzle was also applied to account for radial-flow losses to the exit velocity.

Equation (B1) then becomes

$$F_r = \left(\lambda C_d \frac{\dot{W}_{t,\,id}}{g}\right) V_{ex} + (p_{ex} - p_o) A_{ex} \tag{B2}$$

The thrust coefficient by definition is the result of division of the thrust equation by the product of throat total pressure and throat area.

$$C_{F,\,r,\,\lambda} = \frac{F_r}{P_c^* A_t} = \left[\frac{\lambda\left(\frac{C_d \dot{W}_{t,\,id}}{g}\right)}{P_c^* A_t}\right] V_{ex} + \left(\frac{p_{ex}}{P_c^*} - \frac{p_o}{P_c^*}\right) \frac{A_{ex}}{A_t} \tag{B3}$$

The vacuum thrust coefficient efficiency thus becomes

$$\eta_{C_{F,v}} = \frac{C_{F,v,r}}{C_{F,v,id}} = \frac{\lambda C_d C_{F,d} + \epsilon_{ex}\left(\frac{p_{ex}}{P_c^*}\right)}{C_{F,d} + \epsilon_{ex}\left(\frac{p_{ex}}{P_c^*}\right)} \tag{B4}$$

Two numerical examples of the use of equation (B4) are given for the 1.3-expansion-ratio, contoured-throat conical nozzle and the 2.0-expansion-ratio, tubular-throat conical nozzle. Both nozzles had 15° half-angles of divergence $\lambda = 0.983$ and were operated at an oxidant-to-fuel ratio of 2.0.

Example 1. - Contoured-throat nozzle $\epsilon_{ex} = 1.3$, $C_{d,tc} = 0.994$

$$\eta_{C_{F,v}} = \frac{(0.983)(0.994)(0.992) + 1.3(0.26788)}{0.992 + 1.3(0.26788)}$$

$$\eta_{C_{F,v}} = 0.983$$

For a contoured throat and $\epsilon_{ex} = 2.0$, the thrust coefficient efficiency is 0.981.

Example 2 - Tubular-throat nozzle $\epsilon_{ex} = 2.0$, $C_{d,tt} = 0.977$

$$\eta_{C_{F,v}} = \frac{(0.983)(0.977)(1.207) + 2.0(0.13189)}{1.207 + 2(0.13189)}$$

$$\eta_{C_{F,v}} = 0.9675$$

Note that the degradation of thrust coefficient efficiency for the second example is due entirely to the tubular throat and not to the expansion process, per se.

REFERENCES

1. Salmi, Reino J.; Wong, Alfred; and Rollbuhler, Ralph J.: Experimental Evaluation of Various Nonmetallic Ablative Materials as Nozzle Sections of Hydrogen-Oxygen Rocket Engine. NASA TN D-3258, 1966.

2. Rollbuhler, R. James: Experimental Investigation of Rocket-Engine Ablative-Material Performance After Postrun Cooling at Altitude Pressures. NASA TN D-1726, 1963.

3. Peterson, Donald A.; and Meyer, Carl L.: Experimental Evaluation of Several Ablative Materials as Nozzle Sections of a Storable-Propellant Rocket Engine. NASA TM X-1223, 1966.

4. Rowley, R. W.: An Experimental Investigation of Uncooled Thrust Chamber Materials for Use in Storable Liquid Propellant Rocket Engines. Rep. No. TR-32-561 (NASA CR-53367), Jet Propulsion Lab., California Inst. Tech., Feb. 15, 1964.

5. Tick, S. J.; Hudson, G. R.; and Griese, R.: Design of Ablative Thrust Chambers and Their Materials. J. Spacecraft Rockets, vol. 2, no. 3, May-June, 1965, pp. 325-331.

6. Hughes, T. A.: New Concepts in Ablative Chambers for High-Performance Liquid Rocket Engines. Paper Presented at the AIAA Propulsion Joint Specialist Conference, Colorado Springs, Colorado, June 14-18, 1965.

7. Aukerman, Carl A.; and Trout, Arthur M.: Experimental Rocket Performance of Apollo Storable Propellants in Engines With Large Area Ratio Nozzles. NASA TN D-3566, 1966.

8. Bloomer, Harry E.; Antl, Robert J.; and Renas, Paul E.: Experimental Study of Effects of Geometric Variables on Performance of Conical Rocket-Engine Exhaust Nozzles. NASA TN D-846, 1961.

9. Campbell, C. E.; and Farley, J. M.: Performance of Several Conical Convergent-Divergent Rocket-Type Exhaust Nozzles. NASA TN D-467, 1960.

10. Rao, G. V. R.: Evaluation of Conical Nozzle Thrust Coefficient. ARS J., vol. 29, no. 8, Aug. 1959, pp. 606-607.

11. Elliott, David G.; Bartz, Donald R.; and Silver, Sidney: Calculation of Turbulent Boundary-Layer Growth and Heat Transfer in Axi-Symmetric Nozzles. Rep. No. TR-32-387, Jet Propulsion Lab., California Inst. Tech., Feb. 15, 1963.

12. Zucrow, Maurice J.: Aircraft and Missile Propulsion. Vol. II. John Wiley and Sons, Inc., 1958, p. 450.